https://doi.org/10.5194/egusphere-2026-835
Preprint. Discussion started: 16 February 2026

Quantifying soil organic carbon stocks above the treeline in the Swiss Alps

Michael Zehnder[1,2,4], Annegret Udke[3,5], Katrin Meusburger[5], Frank Hagedorn[5], Andri Baltensweiler[5], Christian Rixen[1,4]

1 – WSL Institute for Snow and Avalanche Research SLF, Davos, Switzerland
2 – Institute of Integrative Biology, ETH Zurich, 8092 Zurich, Switzerland
3 – Department of Geography, University of Zurich, 8057 Zurich, Switzerland
4 – Climate Change, Extremes and Natural Hazards in Alpine Regions Research Centre CERC, Davos Dorf, Switzerland
5 – Swiss Federal Institute for Forest, Snow and Landscape Research (WSL), 8903 Birmensdorf, Switzerland

Correspondence to: Michael Zehnder (michael.zehnder@slf.ch)

Abstract. More than 90 % of the total carbon (C) in alpine ecosystems is stored belowground, yet spatial estimates of soil organic carbon (SOC) stocks remain scarce due to limited accessibility and the demanding nature of SOC stock estimates in rocky alpine terrain. By combining new measurements at 144 sites across the Swiss Alps with data from existing inventories, we compiled a comprehensive dataset on SOC stocks totalling 307 sites from treeline to the permafrost region (1750 m – 3100 m a.s.l.). We predicted the spatial distribution of SOC by linking stock measurements to environmental covariates using Quantile Regression Forests (QRF) and produced a SOC stock map at 25 m resolution illustrating the spatial SOC variability in alpine terrain. Our results show that SOC stocks average 7.3 ± 3.3 kg m^{-2} in alpine grasslands and 1.8 ± 1.7 kg m^{-2} in partly vegetated areas around and above the vegetation line. Overall, the alpine region of Switzerland, which covers one-third of the total country area, stores an estimated amount of 47.6 Mt SOC, representing a non-negligible share of the Swiss greenhouse gas inventory. Vegetation productivity, represented by the Normalized Difference Vegetation Index (NDVI) and topo-climatic covariables, together with vegetation-derived indicators of humus content and soil pH, were highly informative for spatial predictions. This study identifies hotspot regions of SOC storage and influential spatial predictors of its distribution, providing a quantitative baseline for assessing the status-quo and future changes in alpine SOC stocks under continued climate and land-use change. The observed increase in SOC stocks with increasing NDVI suggests that climate change-driven greening at high elevations, where vegetation cover is currently sparse, may enhance SOC storage, although the rates and magnitude of these changes require further investigation.

Keywords: Carbon stocks, soil, alpine, random forest, quantile regression forest, map, modelling, pedotransfer function, digital soil mapping, uncertainty map

https://doi.org/10.5194/egusphere-2026-835
Preprint. Discussion started: 16 February 2026

1 Introduction

Worldwide, cold regions bear the greatest soil organic carbon (SOC) pool in terrestrial ecosystems, with the majority being stored across the northern circumpolar regions (Hugelius et al., 2014; Jobbágy & Jackson, 2000). Whereas at high latitudes, organic matter stocks from arctic soils are well documented (Bockheim & Munroe, 2014; Hugelius et al., 2013; Ping et al., 2008; Siewert, 2018; Wagner et al., 2023), the amount of SOC stored in alpine regions is poorly known due to the difficulty of accessing as well the high heterogeneity of rocky soils (Hagedorn et al., 2019). Yet, mountain regions, covering almost 30 % of the surface area worldwide, provide a variety of ecosystem services (Grêt-Regamey & Weibel, 2020; Ioan et al., 2025) and are expected to be most strongly affected by climate change, with profound consequences for species distributions and ecosystem functions such as carbon (C) storage (Hagedorn et al., 2019; Pepin et al., 2022; Steinbauer et al., 2018; Trautmann et al., 2023).

As global temperatures rise, alpine regions are experiencing shifts in vegetation dynamics, commonly referred to as "alpine greening" (Choler et al., 2021, 2024; Rumpf et al., 2022). Alpine greening could significantly influence C cycling within these ecosystems, due to greater C input through roots and litter, potentially leading to C gains (Quan et al., 2024), particularly above the current vegetation line, where the potential to sequester additional C is high (Udke et al., submitted). However, future sink function may be counteracted by enhanced microbial respiration, driven by warmer temperatures, resulting in higher SOC-derived CO_2 release (Bright et al., 2025; Y. Chen et al., 2024; Hagedorn et al., 2010). As alpine permafrost warms and thaws, SOC may become subject to mineralization, including C release from mineral-stabilized C pools that are considered relatively resistant to decomposition (J. Chen et al., 2020; Streit et al., 2014). Given the large uncertainty in the net-response of alpine SOC stocks to warming and vegetation shifts, there is an urgent need for a baseline assessment of existing SOC stocks in alpine landscapes, especially across elevational gradients and vegetation transitions.

The magnitude and spatial distribution of SOC stocks are shaped by the combined influence of vegetation, climate, topography, parent material, and time, with their interactions often leading to overlapping and complex effects on SOC patterns across the landscape (Baruck et al., 2016; Bonfanti et al., 2025; Guidi et al., 2025; Jenny, 1946; Wiesmeier et al., 2019; R. Yang et al., 2015; Y. Yang et al., 2008). Input of SOC is primarily regulated by vegetation productivity and biomass turnover, while the long-term stabilization of SOC is constrained by microbial decomposition processes and the availability of reactive mineral surfaces linked to parent material (Fang et al., 2019; Jia et al., 2024; Maier et al., 2025; Rowley et al., 2018). Alpine grasslands above the treeline are typically SOC rich, because low temperatures suppress microbial decomposition while dense root systems of perennial alpine plants and leaf litter continuously supply organic inputs to the soil (Peng et al., 2025; Trautmann et al., 2023). In contrast, sparsely vegetated habitats at higher elevation with poorly developed soils on unconsolidated scree material currently store little SOC, and stocks drop abruptly at the vegetation line (Udke et al., submitted). However, these zones have shown the strongest increases in plant productivity and vegetation cover under ongoing warming (Choler et al., 2021). Alpine species can readily colonize such areas under an alpine greening scenario, where loose substrate allows for rooting and organic matter retention. Exposed bare rock, however, impedes colonization due to the lack of physical soil development (Figure 3). Therefore, distinguishing these three major land-cover types (alpine grasslands versus partly vegetated scree and bare rock) is essential for quantifying current SOC stocks and assessing how C storage potential may shift across these early-successional alpine ecosystems.

Numerous soil property maps are available for most low elevation regions of Switzerland (Gupta et al., 2024; Reusser et al., 2023; Stumpf et al., 2023, 2024). Explicit spatial estimates of SOC stocks in Switzerland exist for forest soils (Baltensweiler et al., 2021;

https://doi.org/10.5194/egusphere-2026-835
Preprint. Discussion started: 16 February 2026

Nussbaum et al., 2014; Perruchoud et al., 2000), and for agricultural land (Leifeld et al., 2005; Stumpf et al., 2018). Regarding SOC stocks in alpine regions, earlier efforts such as Zollinger et al. (2013) linked SOC data from a limited number of topsoil profiles to the elevational distribution of permafrost. Leifeld (2005) estimated that alpine pastures contain about 6.3 kg m^{-2} of SOC, while another study with a limited number of soil profiles reported 5.5–10.2 kg m^{-2} for the uppermost 30cm of natural alpine grasslands (Budge et al., 2011). For comparison, Swiss forest mineral soils store around 12.6 kg C m^{-2} (Nussbaum et al., 2014), and permanent lowland grasslands and arable soils contain approximately 9 kg m^{-2} (Leifeld et al., 2005), highlighting the comparatively high SOC stocks stored in alpine ecosystems. However, efforts to quantify the spatial distribution of SOC stocks are constrained by limited sampling density and sampling depth alongside a low economic interest in these regions. A recent study by Udke et al. (*submitted*) addressed this limitation by extensively sampling soil pits down to parent material along elevational gradients from the treeline to permafrost regions. While their study presents the most detailed quantification of the elevational distribution of alpine SOC stocks, a comprehensive spatial SOC stock assessment remains absent for the Swiss Alps. Furthermore, improving the spatial quantification of SOC through adequate sampling density in alpine regions would strengthen national C accounting, which is part of Switzerland's mandatory greenhouse gas reporting under the Paris Agreement (FOEN, 2025).

To quantify SOC stocks across the alpine landscape, we collected topsoil SOC stock data (0-20 cm) at 147 sites distributed throughout the Swiss Alps and complemented this data with existing soil inventory data from Biodiversity Monitoring Switzerland (BDM), capturing the topographic and environmental variability. We further incorporated data from several summit surveys of the Global Observation Research Initiative in Alpine Environments (GLORIA) (Adamczyk et al., 2019), extending coverage into high-alpine and sparsely vegetated summit zones resulting in a total of 307 sites. To estimate SOC stocks beyond the sampled depth of 20 cm, we established pedotransfer functions (PTF) based on depth-dependent distributions of soil variables down to bedrock by Udke et al. (*submitted*). We then developed a predictive spatial model using Quantile Regression Forest (QRF), integrating topographic, climatic, and vegetation-derived covariates, to model SOC stocks on an alpine-wide scale, addressing the question: How much SOC is stored in the alpine soils of Switzerland on an areal base (kg m^{-2}) and in the entire alpine zone (Mt C)? What are informative spatial predictors for SOC stocks, what are the differences among major landcover zones and what is the spatial distribution? In light of the pressing need for robust spatial data on alpine SOC, we provide a comprehensive assessment of SOC stocks based on in-situ data from the treeline to permafrost regions in the Swiss Alps.

2 Materials and Methods

2.1 Study area

The study area covers the alpine region of Switzerland located above the climatic treeline, roughly extending from 1750 m a.s.l. to the nival zone with permanent snow and ice cover. This region is characterized by pronounced climatic gradients resulting from its highly heterogeneous topography. Mean annual air temperature ranges from approximately 1.2 °C, measured at the long-term Stillberg treeline research site (2090 m a.s.l) (Lechler et al., 2024) to about -7 °C as measured at the high-alpine Jungfraujoch climate station at 3571 m a.s.l. (MeteoSchweiz, 2024). The northern Alps have a humid oceanic climate with about 1200-2000 mm of precipitation, while the central Alps have a continental regime with 500-900mm (MeteoSchweiz, 2022). Geological parent material varies substantially throughout the Swiss Alps: while calcareous substrates dominate the Pre-Alps and parts of southeastern Switzerland, metamorphic and crystalline rocks are more common in the Central and Southern Alps, giving rise to a complex mosaic of parent materials and strong variation in soil-forming factors. Soil types across the Swiss alpine region are

https://doi.org/10.5194/egusphere-2026-835
Preprint. Discussion started: 16 February 2026

predominantly Cambisols and Podzols around the treeline to Cryosols, Rankers, Rendzinas and Leptosols at the vegetation line and above (Baruck et al., 2016; Bednorz et al., 2000; Musso et al., 2019).

2.2 Soil sampling campaigns

The soil data originate from three sampling campaigns conducted in the Swiss Alps spanning elevations from 1,750 to 3,150 m a.s.l. covering the entire environmental space of the alpine region. (1) We collected soil data at 97 sites of the Intercantonal Measurement and Information System (IMIS), a climate station network established across the Swiss Alps in the late 1990s located mostly on remote plateaus or gentle slopes to improve avalanche forecasting (Rhyner et al., 2002). To increase topographic heterogeneity, we complemented the IMIS data further with 47 additional sites sampled along five elevational transects, targeting steeper slopes, higher elevations, and calcareous bedrock areas, which were underrepresented in the IMIS dataset. We placed two elevation gradients on calcareous bedrock and three on siliceous bedrock with approximately 175 m elevational difference between sites. Since sampling at the elevational transects followed the same protocol as at the IMIS stations, we refer to them collectively as "IMIS" throughout the study, resulting in a total of 144 sites within this campaign (n_{IMIS} = 144). (2) The second dataset (n_{BDM} = 143) originates from the national soil survey of the Swiss Biodiversity Monitoring programme (BDM), which follows a grid-based sampling design (for details, see Reusser et al., 2023), whereby we filtered the BDM data for sites above 1750 m a.s.l. (3) A detailed methodological comparison supporting the combination of BDM and IMIS data is provided in Appendix C. The third dataset (n_{GLORIA} = 20) stems from mountain summits included in the GLORIA mountain research initiative (Adamczyk et al., 2019), providing SOC stock data for high elevation sites on summits above 2500 m a.s.l. Samples were taken at six different summits in each cardinal direction approximately 10 - 15 m below the summit, resulting in 20 sites, following the GLORIA protocol (Pauli et al., 2015).

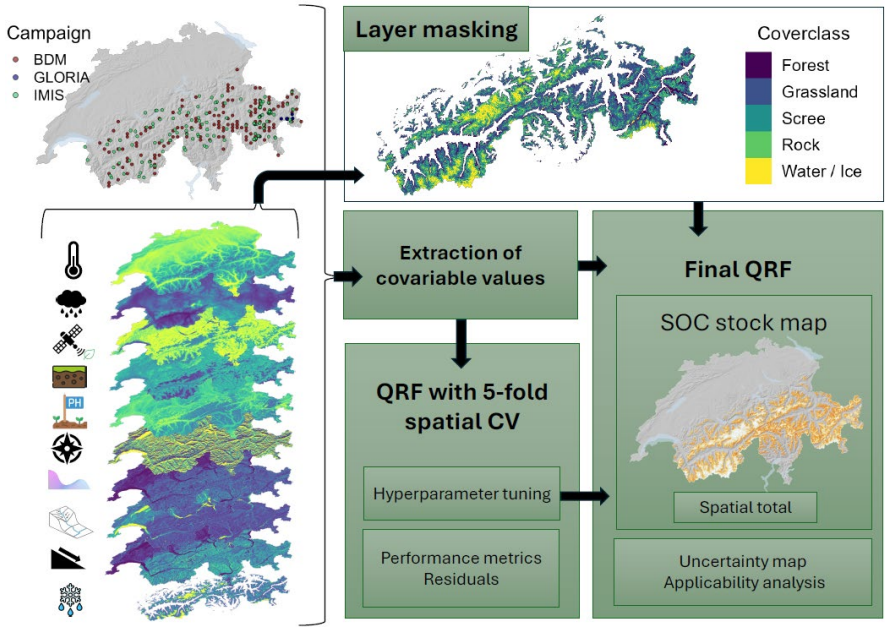

Figure 1: Schematic overview of the workflow. Topsoil data from three monitoring campaigns; Biodiversity Monitoring Switzerland (BDM), Global Observation Research Initiative in Alpine Environments (GLORIA), and the Intercantonal Measurement and Information System (IMIS)

https://doi.org/10.5194/egusphere-2026-835
Preprint. Discussion started: 16 February 2026

including soil profile sites (Udke et al., submitted). Corresponding values of ten environmental covariables available at the national scale (mean summer air temperature, mean precipitation, vegetation greenness derived from the NDVI, vegetation-derived humus-proxy (Landolt-H), vegetation-derived topsoil pH-proxy (Landolt-R), northness, curvature, TWI, slope, and melt-out day) were extracted at each sampling location and used to train a QRF model with 5-fold spatial cross-validation (CV), where hyperparameters were optimized and performance metrics obtained. The final QRF model based on optimal hyperparameters was applied to the masked covariates to generate spatial SOC stock predictions as well as associated uncertainty maps, and to calculate the total spatial SOC stocks.

Three of the five elevation gradients within IMIS included soil pits reaching the parent material, to sample complete SOC profiles from treeline to permafrost regions (1998 m – 3120 m a.s.l.) (Udke et al., submitted). In total, 17 soil pits were excavated, including 5 on calcareous, and 12 on siliceous bedrock. In these soil pits, soil samples of large volumes were taken, allowing us to quantify soil mass and stone content to a greater accuracy compared to topsoil sampling. These profile data were then used to constrain pedotransfer functions (PTF) to quantify the subsoil SOC stocks below 20 cm at all 307 sites used for spatial modelling (Figure 2).

2.3 Estimation of fine earth (FE) density and rock fragment fraction

Estimation of fine earth bulk density (referred to as "fine earth density": FE density) and rock fragment fraction was conducted in the same way in all campaigns, although we acknowledge that potential discrepancies may arise due to different sampling volumes (Figure C2). Soil samples at IMIS sites were taken using a lightweight custom-made metal corer (diameter 2 cm), suitable for sampling in remote areas with difficult access. At each of the sites, we took four spatial replicates with each of them pooled from three cores sampling soils at the depth intervals 0-5, 5-10, and 10-20 cm (Figure 2, Figure C3). For BDM samples, four replica samples were collected using a Humax corer (Martin Bruch AG, Rothenburg, Switzerland) with a diameter of 4.8 cm to a target depth of 20 cm. Given that GLORIA summit soils are typically shallow and rocky, soil samples were collected by excavating four standardized 5 × 10 × 10 cm cubes in each of the four cardinal directions. In all sampling campaigns, four replicates were taken plumb vertically per site, and the organic layer was removed prior to soil sampling. In cases where the soil cores or cubes could not reach the full target depth (e.g. due to stones) of 20 cm for IMIS and BDM, or 5 cm for GLORIA, respectively, the sampled depth was noted, the unprobed portion was conservatively assumed to consist of rock and added to the rock fragment fraction of the probed part of the corresponding soil column. Oven-dried samples (60°C) were sieved into coarse rock fragments (>2mm), roots, and FE (<2mm). FE density was calculated as the mass of dry FE (<2mm) per volume of FE, by subtracting the volume of the coarse rock fraction (>2mm) from the sampling unit volume (Poeplau et al, 2017), assuming a rock density of 2.7 g cm^{-3} for all campaigns. The rock fragment fraction (>2mm) is the volume-percentage of rock (free of SOC) per sampling unit.

2.4 Estimation of SOC stocks for topsoil stocks (<20 cm)

SOC concentrations ($SOC_{\%}$) of the FE were quantified using an automated elemental analyser (Euro EA 3000, Euro Vector, Germany) coupled with a continuous flow isotope ratio mass spectrometry (IRMS, Delta C advanced, Thermo Fisher Scientific Inc., USA) after the FE was milled and homogenized using a ball mill (Retsh, Germany). To calculate $SOC_{\%}$ at (1) BDM sites, the carbonate content was subtracted from the total C content (Gubler et al., 2018), whereby the total carbonate content was determined using hydrochloric acid according to the Agroscope $CaCO_3$ reference method (Agroscope, 2020; Reusser et al., 2023). For IMIS and GLORIA sites on calcareous bedrock, FE samples were acid fumigated to remove inorganic C contents (Walthert et al., 2010).

SOC stocks were collectively determined by multiplying $SOC_{\%}$ with FE density estimates (g cm^{-3}) and the depth of the sampling unit, corrected by the rock fragment fraction for each depth interval *i* (*Eq. 1*) (Poeplau et al., 2017).

https://doi.org/10.5194/egusphere-2026-835
Preprint. Discussion started: 16 February 2026

$$SOC\ stock_i = SOC_{\%} \times Fine\ earth\ density \times depth_i \times (1 - rock\ fragment\ fraction) \quad \textbf{Eq. 1}$$

If applicable, SOC stocks of depth intervals *i* were vertically aggregated for each of the replica, and a mean across all four replica was taken per site. The C stored in roots was not considered in the calculation of SOC stocks. A direct comparison of SOC stocks derived from soil cores and those measured in the uppermost 20 cm of excavated soil profiles showed very high correlation between the two approaches (Figure C1b).

2.5 Pedotransfer functions (PTF) for subsoil SOC stocks (>20 cm)

SOC stocks for deeper soil layers (>20 cm) were estimated by adding depth-extrapolated subsoil stocks to the measured topsoil stocks (0–20 cm). Extrapolation was done using PTF derived from $SOC_{\%}$, FE density, and the rock fragment fraction measured at the 17 soil profiles from three elevational transects on different bedrock (12 on silicious, 5 on calcareous bedrock) (Udke et al., *submitted*), which extended to approximately 60-80 cm depth down to parent material (Appendix B). PTF were applied to topsoil site data using soil properties from corresponding profile sites stratified by bedrock type (calcareous vs. siliceous) and elevation bands (±200 m of the top-soil target site's elevation) that correspond to the topsoil target site. These selected profiles were used to parameterize site-specific depth functions fitting the exponential decline of $SOC_{\%}$, and linear increases of the FE density and the SOC-free rock fragment fraction (for details, see Appendix B). For each topsoil site, we fitted PTFs from two to six different profile sites, that matched the topsoil site with respect to bedrock and elevation and selected the best-fitting PTF for each variable in *Eq. 1* based on the least-squares method (Figure B5). SOC stocks for the subsoil layers were then calculated at 1 cm resolution according to *Eq. 1*, vertically aggregated within 10 cm depth intervals, and added to the measured topsoil stocks. To validate the overall stocks obtained by the PTF approach, we compared modelled against measured values from corresponding profile data for 17 sites where topsoil cores and profiles were sampled (Figure C1a).

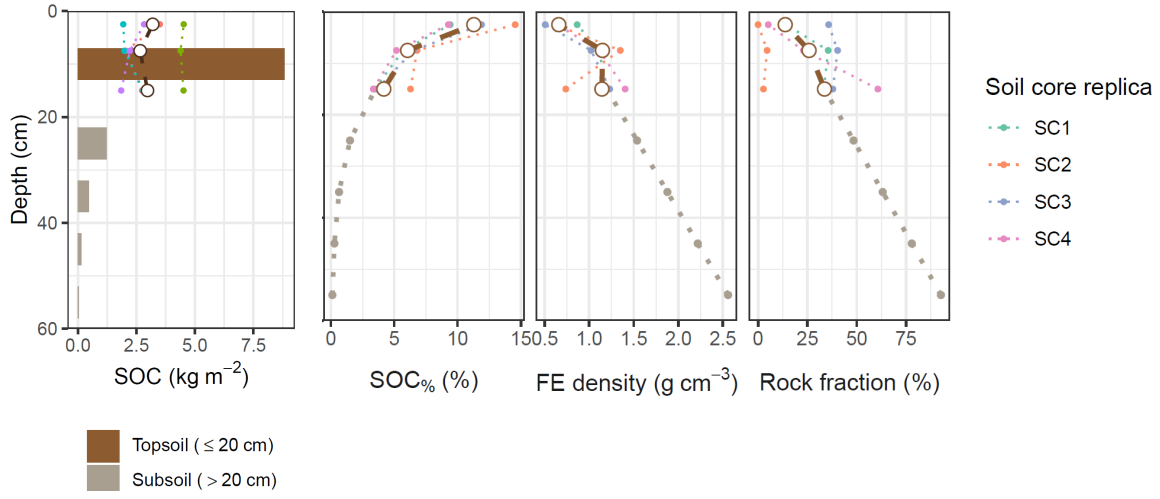

Figure 2: Measured and PTF-modelled SOC stocks and soil properties at an exemplar IMIS site BOG2, 2299 m a.s.l. The left panel shows SOC stocks calculated from measured- and PTF-modelled data. Depth-aggregated SOC stocks (kg m^{-2}) for each soil layer are shown as bars, distinguishing measured topsoil stocks (≤ 20 cm; brown) from subsoil stocks derived from PTF-models (> 20 cm; grey). Stocks were calculated from the variables SOC concentration ($SOC_{\%}$), fine earth (FE) density, and rock-fragment fraction shown in the right panels based on *Eq. 1*. For the upper 20 cm, small points represent measured values from soil-core replicates (SC1–SC4), while large points indicate depth-interval means

https://doi.org/10.5194/egusphere-2026-835
Preprint. Discussion started: 16 February 2026

for 0–5, 5–10, and 10–20 cm. For the subsoil below 20 cm, grey dotted lines represent the PTF-modelled depth functions, while grey points indicate the mid-interval values used to calculate subsoil SOC stocks.

2.6 Spatial covariates

We selected six covariates for predicting SOC stocks based on a priori hypotheses, while scale-dependent topographic variables were evaluated using a multiscale approach (Behrens et al., 2010; Lamichhane et al., 2019). A priori variables were selected based on their expected influence on soil formation and SOC dynamics according to Jenny (1946), which describes soils as a function of climate, organisms, relief, parent material, and time (Table A1). Mean summer temperature (2 m above ground, averaged over the summer months June-August) and mean daily precipitation (average from 1981-2010) was derived from CHELSA high resolution climatologies for Switzerland at 90 m resolution (Zilker & Karger, 2025), representing the climatic soil-forming factor. The period from June to August was chosen to minimize confounding effects of snow cover, as this period represents the period of maximum snow-free extent in alpine terrain. The soil-forming factor "organisms" was captured using the Normalized Difference Vegetation Index (NDVI). NDVI was derived at 25 m resolution from Sentinel-2 scenes and aggregated into a median summer mosaic (June–August) for the period 2015–2018 after cloud and shadow correction in the Google Earth Engine environment (Copernicus/S2_SR). NDVI reflects vegetation greenness and productivity and has been recognised as a strong predictor for SOC (Gomes et al., 2019; Lamichhane et al., 2019).

Furthermore, the length of the vegetation period, which is closely linked to the duration of the winter snow cover in alpine ecosystems, relates directly to primary production (Choler, 2015) and thus the amount of above-ground litter input over the vegetation season. The snow-covered period also influences the frequency and intensity of freeze–thaw cycles, which in turn constrain microbial activity and the transformation of litter into SOC (Gavazov et al., 2017; Perez-Mon et al., 2022). We therefore included a spatial snow melt-out covariable with averaged melt-out dates between 2011–2022 at 30 m resolution computed for areas above 1750 m asl (Bayle et al., 2025).

Parent material has direct effects on weathering, soil formation, mineral composition and thus SOC stocks (Bonfanti et al., 2025; Lamichhane et al., 2019; Trautmann et al., 2023; Wiesmeier et al., 2019). As detailed spatial information of the surface (quaternary) geology is not available for Switzerland, we incorporated a national-scale topsoil pH indicator map from Descombes et al. (2020) at 93 m resolution to approximate bedrock and pH characteristics. The map is derived from plant community composition and associated ecological indicator values (Landolt et al., 2010), using millions of individual georeferenced plant species records to infer underlying soil-chemical properties. It has been empirically demonstrated that Landolt-R (reaction value) correlates strongly with in-situ soil pH by linking community-weighted Landolt-R values to different soil databases (Descombes et al., 2020; Meuli et al., 2017). We further used a humus-indictor map, developed in the same way from plant observations and their respective Landolt-H (humus value), which represents a plant species' preference for humus content, and thus may serve as a suitable spatial predictor for SOC.

As opposed to the effect of climate, vegetation, and parent material, relief-related soil-forming factors are inherently scale-dependent. Accordingly, we evaluated a broad suite of topographic covariates from Baltensweiler et al. (2017, 2020) derived from a 25 m digital elevation model using a multiscale approach (Table A2). This procedure has been shown to be beneficial in digital soil mapping (Behrens et al., 2010; Lamichhane et al., 2019). All candidate topographic covariates were grouped into four conceptual feature types: (1) regional terrain, (2) local curvature, (3) slope related attributes, and (4) aspect related attributes. Multiple formulations were considered for each feature type, each computed at several spatial scales using different smoothings

https://doi.org/10.5194/egusphere-2026-835
Preprint. Discussion started: 16 February 2026

(e.g. 2-, 4-, and 8-cell neighbourhoods), amounting to a total of 46 candidates after removing highly collinear variables. To reduce conceptual redundancy, we selected the highest-ranking candidate within each topographic feature type based on node impurity, derived from a model that evaluated all candidate predictors together with the previously defined a priori covariates (Figure A1). The selected topographic predictors were TWI using the System for Automated Geoscientific Analyses (SAGA), Casorati curvature (both computed using an 8-cell smoothing), the average slope of the local terrain, and northness (defined by the cosine of the aspect) (Table A2). The SAGA TWI characterizes potential water accumulation at an intermediate spatial scale, distinguishing hydrologically convergent areas (valleys and basins) from well-drained ridges and slopes. In convergent areas, water accumulation can promote bog and fen formation, with persistently wet conditions reducing mineralization rates and thereby facilitating SOC accumulation (Grabs et al., 2009; Wiesmeier et al., 2014). Casorati curvature expresses the magnitude of local terrain bending, whereby high positive values indicate areas of sharp bending in multiple directions (Minár et al., 2020). As such, it clearly distinguishes sharp, often rocky ridges and peaks from gentler landforms and valley bottoms. Lastly, the average slope reflects terrain steepness and erosion potential, while northness directly relates to areas with reduced solar radiation and thus, on average, lower soil temperatures, limiting decomposition.

In conclusion, we selected six spatial covariates representing the principal soil-forming factors a-priori and complemented this framework with a multiscale evaluation of DEM-derived terrain parameters to identify four additional topographic covariables of importance. To assess potential collinearity among all ten final covariables, we calculated the Variance Inflation Factor (VIF) for each variable using the *usdm* R-package (Naimi et al., 2014), whereby no multicollinearity was indicated. The selected variables are described in detail in Table A1.

2.7 Quantile Regression Forest

Quantile Regression Forest (QRF) (Meinshausen, 2006) models build on the Random Forest (RF) algorithm (Breiman, 2001) and are well established as a reliable approach for achieving high accuracy in mapping soil variables with the key advantage of capturing non-linear covariable relationships (Baltensweiler et al., 2021; Hengl et al., 2015; Lamichhane et al., 2019; Li et al., 2011; McBratney et al., 2003; Minasny & McBratney, 2016). The QRF model for spatial cross-validation was trained using the *ranger* engine (Wright & Ziegler, 2017) within the *caret R*-package (Kuhn, 2008). The data were partitioned into five spatially contiguous folds based on coordinate proximity, such that, in each iteration, 80 % of the data were used for model training and 20 % were held out for spatially independent validation using the blockCV package (Valavi et al., 2019) (Figure A2). Out-of-fold predictions were used to calculate residuals per site, which were subsequently visualized to assess potential spatial patterns of model bias (Figure 8, Figure A5). To better represent low SOC values in very high elevation regions and to reduce bias towards the central range of the training data (G. Zhang & Lu, 2012), pseudo-zeros were weighted by a factor of three during model fitting. Hyperparameter tuning was performed across the full range of possible mtry values using spatial cross-validation to evaluate model performance for each configuration (Figure A3). Model performance was assessed based on out-of-fold predictions using Root Mean Square Error (RMSE), Mean Absolute Error (MAE), and the Coefficient of Determination (R^2). Performance metrics are reported for the hyperparameter combination that minimized prediction error (lowest RMSE) across spatially contiguous folds, which was selected for the final QRF model used for spatial prediction of SOC stocks. We trained the final QRF used for spatial extrapolation of SOC stocks on the entire dataset with the quantreg = TRUE option in the ranger package (Wright & Ziegler, 2017). The relative importance of spatial covariables was evaluated using impurity-based variable importance native to the ranger package and permutation-based feature importance with 200 randomization runs using the *iml* R-package (Molnar et al., 2018). Partial

https://doi.org/10.5194/egusphere-2026-835
Preprint. Discussion started: 16 February 2026

dependence analyses were conducted using the *iml* R package to explore the direction and relative magnitude of the marginal effects of individual covariables on predicted SOC stocks while holding all other predictors constant.

For spatial prediction, all covariables with coarser native resolutions were resampled with bilinear interpolation if needed. This step serves only to harmonize grids and does not create new spatial information. Therefore, the effective spatial detail of the predictions reflects the native resolution of the underlying predictors and the density of field observations. Spatial predictions were generated at 25 m resolution using the *terra* package, with the median (50^{th} quantile) of the predicted conditional distribution used as the final SOC estimate. Lastly, we computed the total stocks for the alpine region and the cover classes grassland, (partly vegetated) scree, and bare rock areas, by spatially aggregating all predictions.

2.8 Model uncertainty

To identify regions where model predictions can be considered reliable, we computed the Area of Applicability (AOA) using the CAST package (Meyer & Pebesma, 2021). The AOA approach quantifies the multivariate similarity between all spatial prediction data and the model's training space via a Dissimilarity Index (DI). Pixels with DI values exceeding the cross-validated threshold are flagged as outside the model's domain, indicating limited representativeness of the training data in those areas (Figure 9a).

Instead of averaging predictions as an ensemble, QRF keeps individual trees and their prediction distribution (Meinshausen, 2006; Vaysse & Lagacherie, 2017). We then computed the 5^{th}, and 95^{th} quantiles (q_{05}, q_{95}) of the prediction spread, whereby the 50^{th} quantile represents the median predicted SOC stock at each pixel. Local accuracy can thus be expressed as the difference between the q_{95} and q_{05} quantiles of this probability distribution at each pixel, representing the range where 90 % of individual tree predictions fall. We approximated the standard deviation (SD) at each pixel from the 90 % prediction interval (i.e. within quantiles q_{95}–q_{05}) assuming a near-normal distribution, where 90 % of predictions lie within ±1.645 SD (*Eq. 2)*.

$$SD \approx \frac{q_{0.95} - q_{0.05}}{2 \times 1.645} \qquad \textbf{(Eq. 2)}$$

The resulting uncertainty map provides a continuous spatial representation of the model uncertainty across the alpine region (Figure 9b)

2.9 Spatial mask and landcover classes

To delineate the treeless alpine zone of Switzerland, we used the topographic landscape model (TLM3D) provided by the Swiss Federal Office for the Environment (Swisstopo, 2024b). The area above 1750 m a.s.l. was subdivided into five areas: (1) forest, (2) alpine grassland, (3) (partly vegetated) scree, (4) bare rock, and (5) water bodies or permanent ice/snow (Figure 1). For this, we reclassified the original landcover categories in the TLM3D the following way: "forest" and "shrubby forest" were combined into forest. Classes such as "scree" and "boulder fields", which may be vegetated by up to 80 % (Swisstopo, 2025), were grouped as (partly vegetated) scree, while "rock" (i.e. exposed, bare rock) was held separate (Figure 3). Areas of glaciers, permanent snow and standing water bodies were combined into a separate group and assumed to not contain any SOC. The remaining area above the treeline was classified as alpine grassland. Heath vegetation above the treeline was included within the alpine grassland class, as no land-cover product is currently available that reliably distinguishes ericaceous shrub belts from alpine grasslands. For details of the reclassification, see Table D1. The 307 sampling sites were distributed across alpine grassland (n = 259), (partly vegetated) scree (n = 37), and exposed bare rock (n = 11). We added a set of expert-led pseudo-zero points (n = 11) located above 3150 m

https://doi.org/10.5194/egusphere-2026-835
Preprint. Discussion started: 16 February 2026

a.s.l. in permanently snow- and ice-covered areas and on bare rock to inform model behaviour in these high-elevation environments as suggested by Wadoux et al., (2020). Sites located within forested areas (n = 21) were excluded from the analysis, and areas assigned to "forest" were removed from the final SOC stock map. This classification allowed a spatially explicit comparison of total SOC stocks across the three distinct alpine landcover types and was used to mask forested areas above 1750 m a.s.l. as well as regions permanently covered by snow and ice.

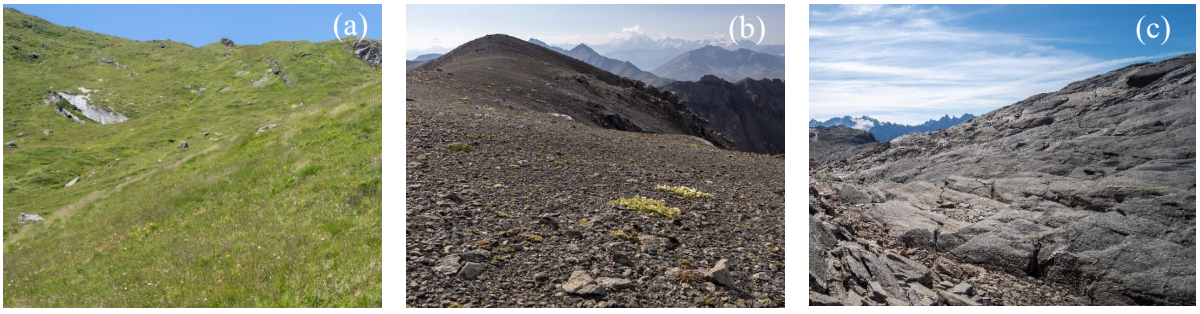

Figure 3: From left to right: a) Alpine grassland dominated by graminoids and forbs on gentle slopes. b) (Partly vegetated) scree. c) Exposed bedrock at high elevation.

3 Results

3.1 Measured SOC stocks

SOC stocks, including measured topsoil stocks and modelled subsoil stocks, ranged from 0.1 to 19.8 kg m^{-2} and varied among landcover classes (Figure 4a, Table A3). All values are reported as mean ± SD. On average, grassland (n= 259) sites stored 7.3 ± 3.3 kg m^{-2}, (partly vegetated) scree (n= 37) contained 1.8 ± 1.7 kg m^{-2} and terrain dominated by bare rock (n=11) contained 1.2 ± 1.4 kg m^{-2} (Figure 4a). Across all sites, the majority of SOC was stored in the upper 20 cm of the soil profile, accounting for 77 % (4.9 ± 2.7 kg m^{-2}) of total SOC stocks down to the parent material (Figure 4b).

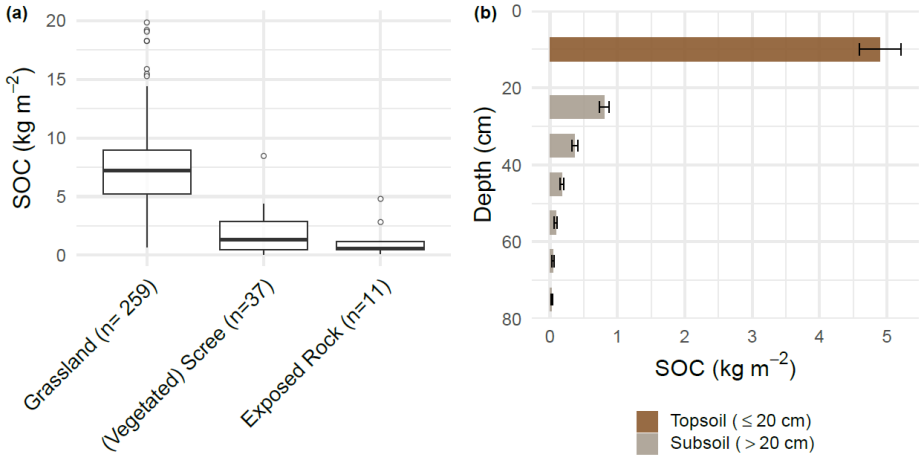

Figure 4: Mean SOC stocks by cover class and depth. a) Differences in SOC stocks among cover classes grassland, (partly vegetated) scree, and areas dominated by exposed, bare rock. b) Vertical distribution of SOC stocks across all sites (n=307). Bar lengths represent mean SOC stocks

https://doi.org/10.5194/egusphere-2026-835
Preprint. Discussion started: 16 February 2026

per depth interval, and error bars show the mean ± 95 % confidence interval. Three quarters of SOC was stored within the top 20 cm (topsoil), with remaining stocks located in deeper subsoil layers modelled using PTF. The depth distributions by cover class are shown in Figure D1.

3.2 Model performance and accuracy

The performance of the QRF model was evaluated using five-fold spatial cross-validation, where geographically separated training and validation subsets were generated using spatial blocking (Valavi et al., 2019). Hyperparameter tuning identified that a minimum node size of 7 and an mtry value of 7 resulted in the best overall performance (Figure A3). Across the spatial folds, the model achieved an R^2 of 0.49 a RMSE of 2.7 kg m^{-2}, and a MAE of 2 kg m^{-2}, indicating a moderate predictive skill fit.

3.3 Relative importance of model predictors

NDVI and Landolt-H, the humus content proxy, emerged as the most influential splitting variable, followed by temperature and Landolt-R, the pH-proxy (Figure 5). While the topographic variables northness and TWI ranked relatively high among topography-related variables, the terrain attributes of curvature and slope ranked among the least important in this impurity-based importance metric. Similarly, precipitation showed a negligable importance among, underscoring temperature and vegetation-derived proxies as more informative for modelling the spatial distribution of SOC. Landolt-R played an important role in partitioning decisions, indicating a meaningful effect of bedrock and surface pH on SOC stocks. Similarly, feature importance analysis based on RMSE loss identified Landolt-H and NDVI as the most important variables for model accuracy (Figure A4). These variables showed distinctly higher RMSE loss (averaged over 200 random permutations) when randomly permutated compared to the next lower ranking covariables Landolt-R, northness and temperature (Figure A4).

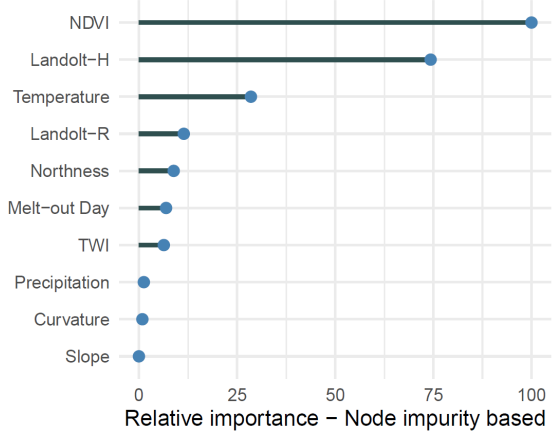

Figure 5: Contribution of covariables to internal tree splitting. The relative importance value shows the total decrease in node impurity attributed to each covariate across all trees relative to the highest-ranking variable. Higher values indicate greater influence on model partitioning decisions.

Partial dependence analyses revealed the direction and relative magnitude of covariate effects on predicted SOC stocks within the QRF, expressed as changes in predicted SOC stocks across the observed range of each spatial covariable while holding all other predictors constant (Figure 6). Predicted SOC stocks increased notably with higher temperatures while the second climatic factor, precipitation, showed only a marginal positive effect. Among topography-related variables, TWI showed the strongest positive association, with higher predicted SOC stocks in areas of hydrological convergence (Figure 6). Northness and slope steepness exhibited a modest negative influence, with marginally higher predicted SOC on more south-facing slopes and lower SOC stocks on steeper terrain. Later snowmelt dates were associated with lower SOC stocks, although the effect was relatively small. Predicted

https://doi.org/10.5194/egusphere-2026-835
Preprint. Discussion started: 16 February 2026

SOC stocks increased strongly with increasing NDVI but levelled off at NDVI values above ~0.65. The Landolt-H (humus indicator) showed a strong positive relationship with predicted SOC stocks and exhibited the widest range of change across its gradient, whereas the Landolt-R (pH indicator) showed a negative relationship and a comparatively narrower range of change with more pronounced effects at the lower end (representing higher pH). These general trends are consistent with the direction of effects observed in the exploratory bivariate relationships between SOC stocks and individual covariables, including the elevational decline of SOC stocks (Figure A7, A8).

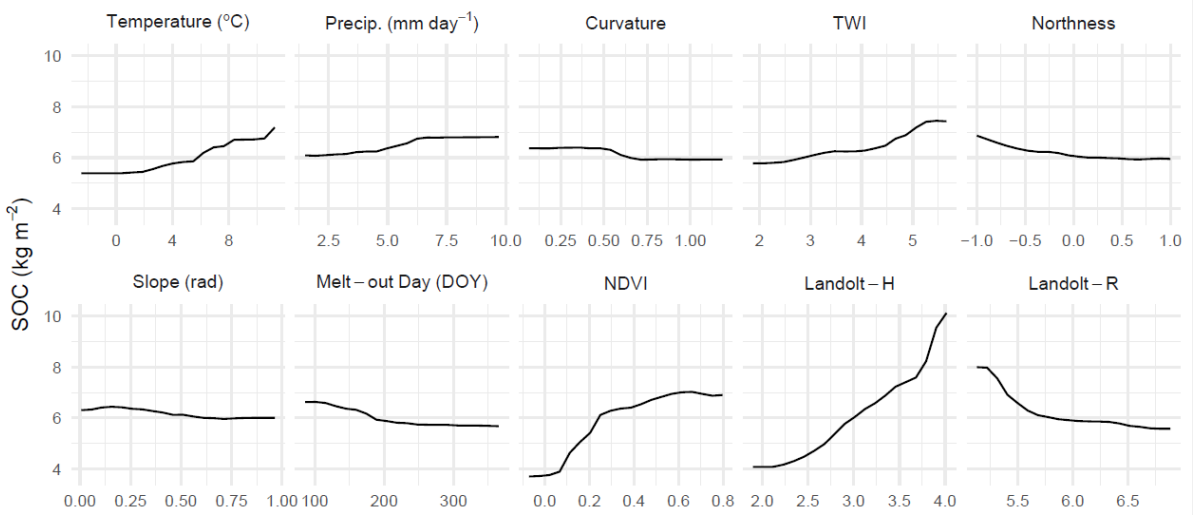

Figure 6: Partial dependence of predicted SOC stocks: Shown are the marginal effects of all covariables: mean summer air temperature and mean daily precipitation, Casorati curvature (magnitude of surface bending), topographic wetness index (TWI), northness (cosine of aspect), slope steepness (in radians), melt-out day of year (DOY) (timing of snow disappearance), NDVI (vegetation greenness), Landolt-H (plant community humus preference), and Landolt-R (plant community reaction value as a proxy for soil pH and parent material). Lines represent the mean partial dependence across all observations, with other predictors held at their observed distributions. The y-axis reflects changes in predicted SOC relative to the QRF model's average response.

3.4 Spatial total and the distribution of predicted SOC stocks

The predicted map of SOC stocks shows a pronounced spatial variability across the alpine region, with higher SOC stocks in the lower alpine belt, and a distinct decrease towards higher elevations (Figure 7). The highest predicted SOC stocks occur just above the treeline and in areas of hydrological convergence. In total, approximately 47.6 Mt of SOC are stored above the treeline (total area: 10'420 km^2), with 34.9 Mt contained in alpine grasslands (mean elevation: 2167 m a.s.l., area: 5'166 km^2) and 6.2 Mt in (partly vegetated) scree (mean elevation: 2520 m a.s.l., area: 2'675 km^2) and 6.5 Mt in areas with exposed, bare rock (mean elevation 2573 m a.s.l, area: 2'578 km^2). For the spatial mapping of SOC stocks, areas corresponding to standing water bodies as well as permanently ice- and snow-covered surfaces were excluded. Consequently, these areas are coloured in icy white in the SOC stock map (Figure 7).

https://doi.org/10.5194/egusphere-2026-835
Preprint. Discussion started: 16 February 2026

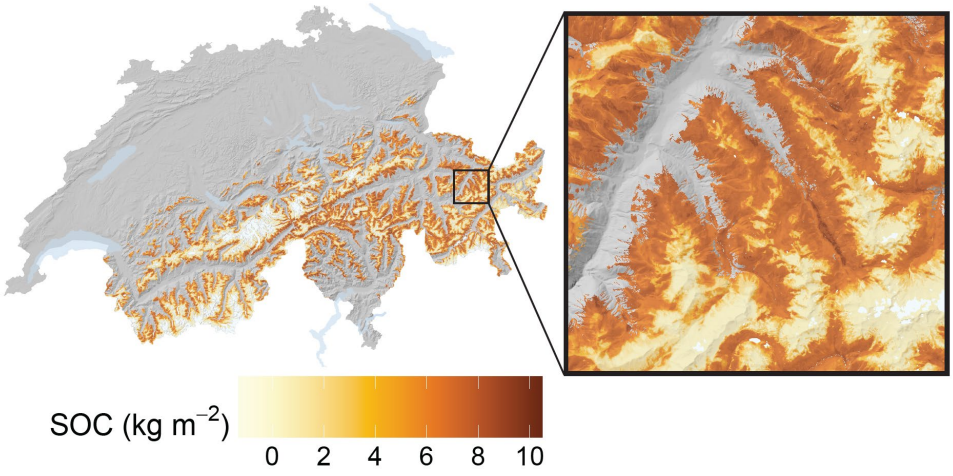

Figure 7: Spatial distribution of modelled SOC stocks above the treeline. Darker brown tones indicate higher SOC stocks. Areas with permanent ice- or snow-covered areas are coloured in icy white. The colour ramp was stretched to ±2 standard deviations around the map-wide mean, with extreme values squished to the scale limits to enhance contrast in the dominant value range.

3.5 Model residuals and uncertainty assessment

Residuals were symmetrically distributed around zero for most sites, with no apparent large-scale spatial clustering (Figure 8). However, a systematic compression of extreme values was evident, where low-SOC stock sites tended to be slightly overestimated and high-SOC sites underestimated (Figure A5a). This pattern reflects the characteristic regression-toward-the-mean behaviour of RF models that arises from averaging predictions across multiple decision trees (Zhang & Lu, 2012). Across the elevational gradient, residuals showed no severe directional bias (Figure A5b), indicating that prediction errors were not systematically related to elevation. However, residual variance tended to decrease with increasing elevation and thus lower measured SOC stocks. Conversely, sites with very high SOC stocks showed larger residuals and a tendency towards underestimation, marked by three extreme outliers with measured SOC stock values of ~20 kg m^{-2} associated with particularly pronounced negative residuals (Figure 8).

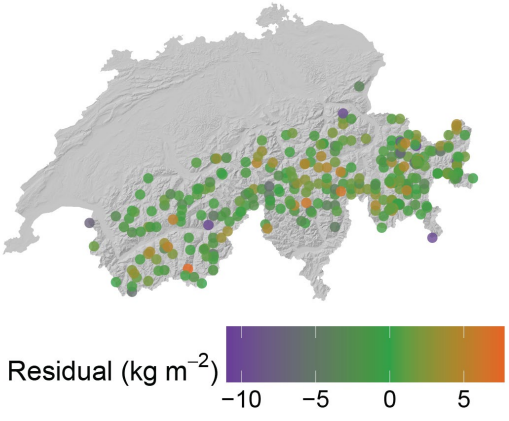

Figure 8: Spatial pattern of prediction residuals (predicted – observed SOC stocks, kg m^{-2}) across all sampled sites. Orange colours indicate overestimation, purple indicates underestimation. Residuals appear spatially random, with no large-scale regional clustering.

https://doi.org/10.5194/egusphere-2026-835
Preprint. Discussion started: 16 February 2026

The AOA analysis revealed that most of the alpine region fell within the environmental space covered by the training data, indicating good applicability of the QRF model (Figure 9a). Regions classified as "not applicable" were mainly located on steep north-facing scree slopes, and areas in the lower Engadin valley (south-east of Switzerland) and the Prealps, where calcareous substrates dominate. Standard errors were generally low to moderate and in line with the RMSE of 2.7 kg m^{-2} across large parts of the alpine region (Figure 9b). The highest standard errors occurred predominantly in zones just above the treeline, where SOC stocks are generally higher, but dropped significantly towards higher elevations (Figure A6, supplementary data: *SD_map.tif*).

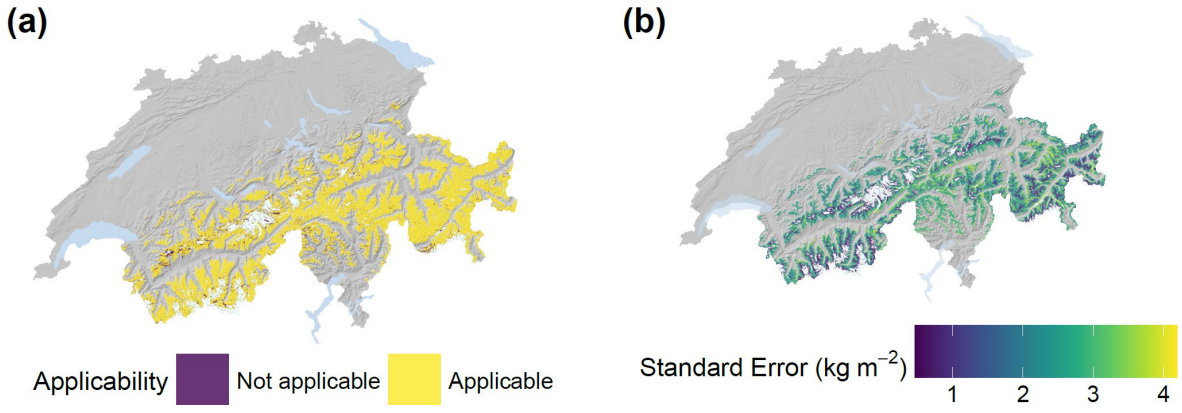

Figure 9: Spatial model applicability and uncertainty. a) Area of applicability (AOA) (Meyer & Pebesma, 2021) of the QRF model predicting SOC stocks across the alpine region of Switzerland. Yellow areas indicate regions where environmental conditions are represented within the model's training space (applicable), whereas purple areas denote extrapolation beyond model's training domain (not applicable). b) Spatial distribution of model uncertainty based on the spread of predictions of the QRF model (Meinshausen, 2006; Michel 2024) for SOC stocks across the Alpine region of Switzerland. Higher, more yellow values indicate areas where the model predictions are less certain, whereas darker areas show greater model confidence. The colour ramp was stretched to ±2 standard deviations around the map-wide mean, with extreme values squished to the scale limits to enhance contrast in the dominant value range.

4 Discussion

In this study, we provide the first spatially explicit estimate of SOC stocks in alpine soils above the treeline in Switzerland, showing distinct decreases in SOC stocks with increasing elevation and decreasing vegetation greenness (NDVI). We estimate that these high-elevation systems store approximately 47.6 Mt of SOC, indicating that alpine soils above the treeline constitute a non-negligible share of the Swiss national SOC pool.

4.1 Alpine SOC stocks in context

We found that measured SOC stocks in alpine grasslands averaged 7.3 ± 3.3 kg m^{-2} (Figure 4a), which is comparable to the range reported by Budge et al. (2011), who estimated 5.5–10.2 kg m^{-2} (0–30 cm) across five typical alpine grassland sites in Switzerland. As expected, SOC stocks generally declined with lower temperatures, reflecting the well-documented decrease in SOC stocks above the treeline in mountain regions (Bonfanti et al., 2025; Hagedorn et al., 2019; Kuhry et al., 2022; Udke et al., submitted) (Figure 6, Figure A8). Our data indicate a non-linear decline of SOC stocks with elevation. While SOC stocks remain almost constant in grasslands up to an elevation of 2500 m a.s.l. (Figure A9), they decrease sharply towards (partly vegetated) scree with average stocks of 1.8 ± 1.7 kg m^{-2}, and further to 1.2 ± 1.4 kg m^{-2} in areas dominated by bare, exposed rock with minimal vegetation

https://doi.org/10.5194/egusphere-2026-835
Preprint. Discussion started: 16 February 2026

cover (Figure 4a). Our measured averages are lower than SOC stocks in Swiss forest soils, which average 12 – 13 kg m^{-2} excluding the organic layer (Guidi et al., 2025; Rogiers et al., 2025). Our averages are also below estimates for permanent (lowland) grassland (9.2 kg m^{-2}) and arable land (9 kg m^{-2}) reported by Leifeld et al. (2004). However, our average of 7.2 kg m^{-2} for all grasslands above the treeline aligns well with their estimate for managed alpine grassland of 6.3 kg m^{-2}.

With an average of 7.2 ± 3.4 kg m^{-2} for alpine grasslands in Switzerland, SOC stocks are lower than those reported for alpine grasslands on the Tibetan Plateau, where reported stocks range from 9–16 kg m^{-2} (Liu et al., 2016; Y. Yang et al., 2008). This contrast likely reflects the younger, less developed soils of the Swiss Alps formed after late-glacial deglaciation, their higher skeletal content (frequently exceeding 50 %; Figure B4), the steeper terrain, and the influence of a more oceanic climate, whereas the Tibetan highlands are characterized by older, more pedogenically mature soils and a more continental climate, where colder conditions slow organic matter turnover. Similarly, permafrost affected soils of the Arctic taiga and tundra, which are typically characterized by thick organic layers, store substantially larger amounts of C, often exceeding 30 kg m^{-2} (Hugelius et al., 2014; Ping et al., 2008; Siewert, 2018). Nevertheless, the data presented here are unique in that spatial SOC stock assessments for mountain regions are still rare.

For areas classified as bare, exposed rock, we measured an average SOC stock of 1.2 ± 1.4 kg m^{-2}, while (partly vegetated) scree sites showed slightly higher values of 1.8 ± 1.7 kg m^{-2} (Figure 4a). These estimates from poorly developed high-elevation soils are consistent with values reported for comparable landscapes in the high central Andes (Kuhry et al., 2022) and for high-latitude mountain soils in North America (Ping et al., 2008). However, sampling in these areas was limited, particularly for sites classified as bare rock (n = 12), as soil collection on predominantly bare rock is often impractical due to the absence of sufficient soil material. Moreover, it is difficult to reliably quantify the small amounts of SOC that may accumulate in rock crevices, originating from sparse cushion plants or isolated alpine specialists. Ancient SOC originating for warmer periods in the Holocene which are buried under stones may additionally contribute to SOC in periglacial environments (Pintaldi et al., 2021). The modest difference between bare, exposed rock and scree thus likely reflects a sampling bias: sites located within the bare rock zone were probably sampled only where substrate was present, thereby overestimating actual stocks in this category. Nevertheless, spatial predictions at high elevation (>3000 m a.s.l.) remain representative, as the inclusion of pseudo-zero observations effectively constrains model behaviour in nival areas where SOC stocks are approaching negligible amounts.

Aggregating spatial SOC stock predictions across the study area, we estimate that approximately 47.6 Mt of SOC are stored above the treeline, corresponding to a total area of 10’400 km^2, of which about 38 Mt are held in alpine grasslands and roughly 7.9 Mt in (partly vegetated) scree (2’000 km^2) and 8.2 Mt in areas dominated by bare, exposed rock (2’600 km^2). For context, Leifeld et al. (2005) reported a spatial total of 36.5 Mt C in managed areas classified as alpine meadows and pastures. However, their estimates only cover agricultural land, whereas our sampling notably extends into sparsely vegetated alpine terrain at higher elevation beyond the agricultural zone, which may explain this higher total stock estimate. All agricultural soils, including lowland areas, were estimated to contain about 2.5 times as much SOC, while Swiss forest soils store roughly three times more SOC than alpine regions (Bolliger et al., 2008; Hagedorn et al., 2018). However, the spatial total of 47.6 Mt SOC stored in alpine soils surpasses the estimated 30 Mt of SOC stored in the remaining organic peat soils in Switzerland, which have lost roughly 80 % of their estimated 203 Mt C since 1850 due to long-term drainage and land-use change (Hagedorn et al., 2018). Thus, SOC stocks above the treeline contribute a non-negligible addition to existing national SOC estimates.

https://doi.org/10.5194/egusphere-2026-835
Preprint. Discussion started: 16 February 2026

4.2 Predictors of SOC stocks

The set of environmental covariates used in the QRF broadly represents the principal soil-forming factors after Jenny (1941): climate (temperature, precipitation and melt-out), organisms (NDVI, Landolt-H), relief (TWI, curvature, northness, slope), and parent material (Landolt-R). The soil-forming factor time and detailed lithological relationships are not explicitly represented, as no adequate spatial data are available at the scale of this analysis. Across the different analytical approaches, NDVI, Landolt-H and temperature consistently ranked among the most influential covariables in the QRF, although their relative ranking varied slightly between node impurity-based and permutation-based variable importance (Figure 5, Figure A4). Impurity-based variable importance quantifies the cumulative reduction in variance of SOC stocks achieved by all splits where a given covariable is used across the forest. Accordingly, NDVI and Landolt-H as a proxy for vegetation productivity and humus content and provide the strongest partitioning of SOC stocks in the model, which indicates that these gradients play a key role in structuring spatial predictions. Temperature ranked as the third most important predictor and reflects the strong elevational temperature gradient characteristic of mountainous regions. Thus, the observed patterns are generally in line with the elevational decline of SOC stocks previously reported for mountainous regions.

The alpine temperature- and elevation gradient alone implicitly integrates a wide suite of soil-forming factors and is inversely related to NDVI. The relationship between above- and below-ground productivity (represented by NDVI in our model) and SOC storage is well documented in East-Asian grassland ecosystems (S. Chen et al., 2018; Peng et al., 2025; Quan et al., 2024; Y. Yang et al., 2008). Aspect (northness) ranked high in node-impurity metrics and even higher in the permutation-based feature importance (Figure A4), with more south-facing slopes associated with higher SOC stocks. This pattern contrasts with previous studies reporting higher SOC stocks on north-facing slopes (Egli et al., 2009; M. Zhang et al., 2025). In our study, this relationship is likely driven by enhanced vegetation productivity on warmer, south-facing slopes (Figure A9), which highlights the role of plant-derived C input in the alpine region, represented by the high importance of NDVI.

The TWI showed a positive association with high predicted SOC stocks (Figure 6) and is known to play a key role in spatial SOC predictions in other regions (Hengl et al., 2015; Lamichhane et al., 2019; Wiesmeier et al., 2014). As an indicator of regional moisture accumulation potential, TWI can highlight areas prone to alpine bog and mire formation, where some of the highest measured SOC stocks in our dataset were measured. In contrast, the comparatively minor influence of slope and curvature in impurity-based importance implies that their effects on SOC are either less pronounced or already captured better by the higher-ranking variables. For instance, Casorati curvature is highest at sharp mountain ridges and may largely be captured by the temperature–elevation gradient. Lastly, precipitation showed only weak relevance in our models, contrasting with findings from more arid regions (e.g. Yang et al., 2008) and Swiss forest ecosystems (Guidi et al., 2025), where higher soil moisture is associated with increased SOC stocks. The limited importance of precipitation in Alpine soils may be attributed to the long lasting snow cover and lower water losses through evapotranspiration, leading to an adequate water supply (Meusburger et al., 2022) and the predominance of well-drained soils along mountain slopes that hinder the development of anaerobic conditions.

The positive relationship between NDVI and SOC stocks and the negative temperature effect that we found above the treeline contrasts with forest ecosystems, where elevation-dependent changes in above-ground productivity and SOC storage are decoupled. As opposed to the studied alpine soils, total SOC stocks in forest soils show minor changes with elevation, and net primary productivity is even negatively correlated with SOC stocks, while mineralogical and geochemical controls of SOC stocks play a more important role (Bramble et al., 2024; Guidi et al., 2025). A recent study within the lower alpine vegetation belt, where

https://doi.org/10.5194/egusphere-2026-835
Preprint. Discussion started: 16 February 2026

biomass production is comparatively uniform relative to the pronounced gradients from the treeline to permafrost-affected regions as in our study, showed that mineralogical control appears to dominate in this elevation belt (Maier et al., 2025). However, in high-alpine ecosystems, soils become increasingly shallow and vegetation cover sparse, and low temperatures strongly constrain decomposition rates and plant growth. Under these conditions, SOC accumulation may be particularly sensitive to plant-derived C inputs (Peng et al., 2025), consistent with the strong role of NDVI observed in our models. At the same time, partial dependence analyses suggest that the positive effect of NDVI on predicted SOC stocks saturates beyond an NDVI threshold of approximately 0.65 (Figure 6). This NDVI range is characteristic of grasslands in the lower alpine belt (c. 2,000–2,300 m a.s.l.) (Figure A9). The plateauing indicates a reduced sensitivity of SOC stocks to further increases in aboveground biomass once a relatively dense cover is established, consistent with the findings by Maier et al. (2025).

Predicted SOC stocks declined with increasing Landolt-R values, indicating lower SOC storage in soils with higher pH, in line with findings from similar studies (Bonfanti et al., 2025; Udke et al., submitted). This pattern can first be explained by pH-dependent microbial processes: acidic conditions on siliceous parent material limit microbial enzymatic activity, whereas higher pH conditions on carbonate bedrock favour microbial decomposition and mineralization of organic matter (Jones et al., 2019; Malik et al., 2018; Wang & Kuzyakov, 2024). In addition, differences in soil mineralogy may contribute to this pattern. Carbonate weathering produces little secondary clay, thereby limiting the availability of mineral surfaces for organo-mineral associations, although calcium-mediated interactions can effectively stabilize SOC in carbonate soils (Rowley et al., 2018). In contrast, in soils developed on siliceous parent materials with lower pH, chemical weathering promotes the formation of secondary clay minerals and Fe- and Al-(hydr)oxides that provide reactive surfaces for organo-mineral associations, facilitating the stabilization and storage of SOC (Fang et al., 2019; Jia et al., 2024; Maier et al., 2025). Both bedrock types are associated with characteristic microbial and plant species communities reflecting their preference for basic or acidic soil chemistry (Adamczyk et al., 2019; Gigon, 1987; Landolt et al., 2010). We acknowledge that we did not use a “true” surface pH covariable, because a reliable spatial product for surface geology and their pH or other detailed geochemical information in alpine regions is yet lacking for Switzerland. We therefore encourage efforts to produce a high-resolution surface pH map for Switzerland, which would support more direct spatial mapping of soil properties. However, we showed that the pH proxy map derived from individual plant occurrences and their respective pH preferences of Descombes et al. (2020) can capture this relationship between bedrock, soil pH and plant community composition on a spatial scale. Indeed, the Landolt-R covariable, a proxy for surface pH, significantly contributed to the model accuracy, although not ranking among the most important variables for tree-splitting (Figure 5). Random permutation of this covariable reduced model RMSE by approximately 1.3 kg m^{-2}, which indicates a substantial contribution to predictive performance. This highlights that, even across a pronounced elevational gradient where NDVI is most informative for SOC predictions, parent material, associated mineralogical controls and pH remain an important mechanistic component of SOC storage.

The vegetation-derived humus indicator (Landolt-H) (Landolt et al., 2010) was very frequently used to partition SOC stocks within the decision trees (Figure 5) and even showed the highest variable importance based on accuracy loss (Figure A4). Ecological indicator values are derived from plant species’ realised niches; in this case, reflecting preferences for humus-rich or humus-poor soil conditions. Accordingly, the high rank in the importance metrics reflects shared variation with SOC rather than an independent mechanistic driver or a controlling factor of SOC. Nevertheless, this result indicates that spatial information inferred from aboveground vegetation composition can improve the performance of spatial SOC models. As the density of georeferenced plant observations from national monitoring programmes and citizen science projects outnumber soil profiles and point measurements by orders of magnitude, the use of vegetation-derived proxies to predict topsoil characteristics on a spatial scale seems reasonable.

https://doi.org/10.5194/egusphere-2026-835
Preprint. Discussion started: 16 February 2026

Future work could assess whether the remaining ecological indicator values mapped by Descombes et al. (2020), such as temperature-, nutrient-, or soil dispersion preference, could further improve the spatial prediction of soil properties, especially when updated with the species occurrence data collected in recent years, including the substantial increase in records during and after the COVID-19 period (InfoFlora, 2024).

4.3 Uncertainties in modelling SOC stocks on a larger scale

Three types of uncertainties commonly encountered in digital soil mapping: (1) Uncertainty from measurement errors in the input data, (2) uncertainty related to the limited size and representativeness of the training dataset, and (3) uncertainty resulting from the fact that the covariates capture only part of the variability in SOC stocks.

Estimating fine-earth density is particularly challenging in alpine soils, where coarse-fragment content, rockiness, and SOC concentration vary substantially over short distances. These challenges are amplified when different sampling volumes are used or when data from multiple campaigns are combined. Even when resampled at the same sites, we sometimes observed differences for SOC stocks between the two sampling approaches, although the tested sites were generally in high agreement ($R^2 = 0.8$) (Figure C2). Nevertheless, to the best of our knowledge, we compiled the most comprehensive SOC stock dataset to date for alpine regions. Sampling densities in comparable high-elevation (or high latitude) studies are typically even lower than in our dataset (e.g. Weiss et al., 2017; Liu et al., 2016). Our sampling encompassed 307 sites, capturing a sufficiently large environmental gradient and allowing for a good model representativeness for the alpine area of Switzerland. Although a sampling density of approximately 33 plots per km² has been suggested for accurately modelling SOC stock distribution in alpine terrain (Hoffmann et al., 2014), this is clearly unrealistic at the national scale. Given our much lower sampling density, a relatively large prediction error can be expected. The RMSE of 2.7 kg m^{-2} obtained from spatially cross-validated test data is thus a reasonable reflection of data limitations and spatial heterogeneity.

Overall model performance was moderate ($R^2 = 0.49$). This indicates that a considerable proportion of SOC stock variability could not be explained by the model and the resulting map, even though the main spatially available predictors expected to influence SOC storage in alpine regions were included. However, model performance was comparable to, or slightly better than, similar modelling approaches used to estimate SOC stocks at larger spatial scales ($R^2 = 0.3–0.5$, depending on the soil depth compartment and ecosystem) (Bui et al., 2009; Gomes et al., 2019; Hounkpatin et al., 2020; Martin et al., 2011; Nussbaum & Burgos, 2021; Wiesmeier et al., 2014), and thus in line with expectations for SOC stock mapping.

The use of PTF allowed us to account for subsoil SOC stocks, which represent about 20 % of the total stocks (Figure 4b). Subsoil stocks are typically difficult to measure directly in the field, especially for remote stony soils at this scale, and therefore, we consider this modelling approach worthwhile. However, the accuracy of PTF-based extrapolation depends on the similarity of local conditions to those represented in the reference dataset of 17 deep soil profiles by Udke et al (*submitted*). Sites to model subsoil stocks were chosen based on best-possible environmental match between each topsoil site and a corresponding soil profile site (Figure B5). While the set of profiles used for PTF cover a large environmental gradient, they do not necessarily reflect the exact in-situ conditions at all topsoil sites, thus introducing an additional model uncertainty, which we did not additionally validate through excavating additional soil pits at randomly picked topsoil sites, as this exceeded the extent and labour of this study. We did, however, compare the stocks measured by soil profiles with the stocks from topsoil cores with added subsoil stocks (modelled through PTF) at the same site, which resulted in very high correlations ($R^2 = 0.91$ for silicious bedrock, 0.86 for calcareous bedrock, Figure C1a), supporting the internal consistency of the PTF approach to model subsoil SOC stocks.

https://doi.org/10.5194/egusphere-2026-835
Preprint. Discussion started: 16 February 2026

To assess uncertainties arising from input data limitations and model representation, we (i) evaluated the spatial distribution of residuals, (ii) produced an uncertainty map based on QRF (Meinshausen, 2006), and (iii) quantified the area of applicability (AOA) following Meyer & Pebesma (2021). The AOA analysis confirmed that most of the environmental space in the alpine zone is covered by our training data (Figure 9a). Conversely, the AOA highlights regions where higher sampling density could further improve the accuracy of alpine SOC stock maps. These are mainly high elevation areas in the northern Pre-Alps, and north-facing scree dominated slopes on calcareous parent material, which could represent priorities for additional sampling in future surveys. (*Supplementary data: AOA.tif)*. Moreover, our dataset includes several samples from carbon-rich bogs and fens, which is reflected in the final SOC map by the pronounced representation of SOC-rich depressions driven by the variable TWI, as illustrated in the local detail maps. These patterns seem to accurately capture areas where bogs and fens occurred (at least historically), although the predicted SOC stocks (~10 kg m^{-2}) are underestimated for such organic-rich soils. This underestimation is partly methodological: QRF provide median predictions, which tend to be lower than mean predictions in strongly right-skewed SOC distributions. As a result, SOC-rich but spatially limited environments, such as mires and valley bottoms, are smoothed towards more typical conditions, leading to conservative estimates in these SOC hotspots. Incorporating additional samples from the remaining alpine mires would allow these fine-scale features to be further refined.

Model residuals were symmetrically distributed around zero for most sites, with no large-scale spatial clustering (Figure 8). Despite higher weights to pseudo-zero values and sites with high SOC stock values in the model training, we observed heteroscedasticity (overestimation of low SOC stocks and underestimation of high ones; Figure A5a). However, this is expected for ensemble tree-based algorithms such as RF models, which inherently regress predictions towards the mean (Meinshausen 2006, Zhang & Lu, 2012). Importantly, this heteroscedasticity does not translate into a severe systematic bias along the elevational gradient: residuals did not show consistent over- or underestimation in low- versus high-elevation areas (Figure A5b), indicating model robustness across the elevational gradient. The few extreme negative residuals correspond to sites with exceptionally high SOC stocks exceeding 15 kg m^{-2}, resulting in a tendency of underestimation in lower regions. The narrowing residual spread with increasing elevation further suggests that uncertainty is smaller where SOC stocks are naturally low and less variable. Because areas with a tendency of underestimation are spatially more extensive (i.e. lower alpine belt) than areas with overestimation towards narrowing mountain peaks, the resulting total SOC stock estimate of 47.6 Mt is likely conservative.

We computed uncertainty maps based on the quantiles of the spread of predictions, which is an important and widely used tool to estimate spatial uncertainty in digital soil mapping (Meinshausen, 2006; Vaysse & Lagacherie, 2017; Wadoux & Heuvelink, 2023). Areas of the lower alpine region showed the highest SD, reaching up to 5 kg m^{-2} (Figure 9b), coinciding with the residual spread of model predictions at out-of-fold sites. This was expected, as SOC variability is substantially higher and more variable at lower elevations. Areas of particularly high uncertainty are concentrated just above and around the treeline and hydrologically convergent terrain with high SOC stock predictions, whereas uncertainty decreases with increasing elevation (Figure A6). Within the alpine grassland belt, which contains the largest share of SOC, SD typically ranges between 2 and 3 kg m^{-2}, consistent with the overall model RMSE of 2.7 kg m^{-2}. The provided uncertainty maps should be taken into account when interpreting the provided SOC stock map.

4.4 Outlook

We observed a decline in SOC stocks with higher elevation and lower NDVI, which highlight the C sink function of alpine soils given that elevation acts as a space-for-time substitute for future warming and greening. There is ample evidence that the alpine regions are experiencing shifting vegetation into higher elevations (Iseli et al., 2023; Steinbauer et al., 2018; Vitasse et al., 2021;

https://doi.org/10.5194/egusphere-2026-835
Preprint. Discussion started: 16 February 2026

Walther et al., 2005), increased productivity (Choler, 2015; Choler et al., 2024; Rumpf et al., 2022), and earlier plant growth (Shen et al., 2022; Zehnder et al., 2025). These changes may facilitate soil formation and SOC accumulation through increased biomass production and C input in high alpine regions that further promotes colonization by upward shifting vegetation – analogous to SOC formation along retreating glaciers or debris flow fans (Egli et al., 2010; Y. Zhang et al., 2023). It was recently suggested that particularly the areas in the sparsely vegetated nival belt could function as emerging C sinks because of currently low C input rates (Udke et al., *submitted*). However, not all high-elevation areas are equally suitable for plant colonization. Loosely aggregated scree and areas dominated by exposed, bare rock each occupy a similar spatial extent (≈ 2,600 km²), yet extensive vegetation greening on bare rock remains limited, effectively excluding some areas to function as substantial C sinks. Future work should therefore aim to identify high-elevation locations with a greater potential for plant colonization, as these areas may represent zones of elevated future C uptake – although limited in spatial extent. In contrast, SOC accumulation in alpine grasslands, which cover extensive areas in the lower alpine belt, is constrained by the availability of reactive mineral surfaces, as high(er) C inputs lead to a high SOC saturation in the soil, thereby reducing their capacity for additional SOC storage (Georgiou et al., 2025). Notably, SOC stocks within the alpine grassland belt show only a weak decline with elevation in the grassland belt, but decrease sharply at the vegetation line (Figure A8). Consequently, alpine grassland soils may be more vulnerable to SOC losses despite potentially higher aboveground C inputs, as observed in accelerated SOC mineralisation near the treeline under experimental warming (Hagedorn et al., 2010; Streit et al., 2014).

This study identified alpine SOC hotspots primarily in areas around the treeline and in hydrologically convergent terrain, such as alpine mires and high-alpine valley bottoms. However, the persistence of such SOC hotspots under future climate change remains uncertain. Rising temperatures, reduced snow cover, and an increasing frequency of summer droughts are expected to promote soil drying, potentially shifting alpine environments that currently experience relatively persistent soil moisture towards intermittently dry conditions (Marty et al., 2017; MeteoSwiss; & ETH, 2025; Richter & Marty, 2026). As a result, SOC stocks that are presently stabilized by cool and moist conditions may become increasingly vulnerable to accelerated C losses, offsetting or even outweighing potential gains above the current vegetation line. How the net C balance will evolve across alpine landscapes over space and time therefore remains an open question and deserves further investigation (Bright et al., 2025).

5 Conclusion

Alpine SOC stocks were estimated using a combination of measured topsoil stocks and extrapolated subsoil stocks based on PTF. Using QRF, we generated the first high-resolution SOC stock map at 25 m for the Alpine terrain in Switzerland, while providing both spatial predictions and associated uncertainty. Our results highlight NDVI, temperature, and ecological indicator maps derived from large plant species datasets as informative spatial predictors for the study region. Overall, alpine SOC stocks were estimated to be 47.6 Mt, whereby an average of 7.3 ± 3.4 kg m^{-2} was stored in alpine grasslands, highlighting the importance of land above the treeline as a major contributor to the total national C inventory, but also the general importance of alpine regions for C storage. How alpine SOC stocks will develop under future warming and greening remains uncertain, though the observed decline in SOC stocks with elevation suggests a C sink function on unconsolidated substrate at high elevation that can be colonized by upward shifting vegetation and associated new input of C into soils.

6 Author contributions

MZ – Conceptualization, Data curation, Formal Analysis, Investigation, Methodology, Project administration, Software, Validation, Visualization, Writing (Original Draft Preparation, Review & Editing); **AU** – Conceptualization, Formal Analysis,

https://doi.org/10.5194/egusphere-2026-835
Preprint. Discussion started: 16 February 2026

Investigation, Methodology, Validation, Writing (Review & Editing); **KM** – Formal Analysis, Software, Investigation, Funding Acquisition, Methodology, Resources, Writing – (Original Draft Preparation, Review & Editing); **FH** – Conceptualization, Funding Acquisition, Investigation, Methodology, Project administration, Resources, Writing (Review & Editing); **AB** – Software, Resources, Methodology, Writing (Review & Editing); **CR** – Conceptualization, Investigation, Funding Acquisition, Methodology, Project administration, Resources, Supervision, Writing (Review & Editing)

7 Supplement links

SOC_stock_map.tif *SD_map.tif* *AOA_map.tif*

8 Code and data availability

Model code and IMIS soil data *will be deposited* in envidat (Zehnder et al., 2026). Profile data from Udke et al (submitted) used for PTF development will be deposited in envidat. BDM and GLORIA soil data are available upon request from the Swiss Federal Office for Agriculture (FOAG) and the GLORIA coordination office, respectively. The sources of environmental data used in spatial models is described in Table A2.

9 Competing interest

One of the co-authors is a member of the editorial board of the journal Biogeosciences. Besides, the authors declare that they have no conflict of interest.

10 Acknowledgements

We specifically thank the contributors of soil data. Namely, soil monitoring data were provided by NABO (Swiss Soil Monitoring Network), a long-term monitoring program funded by the Swiss Federal Office for the Environment (FOEN) and the Swiss Federal Office for Agriculture (FOAG). Further data specifically for mountain summits was provided by the GLORIA team. We also acknowledge the help of various fieldwork and lab helpers and civil service personal, most importantly, Andreas Scharl, Andreas Fichtner, Mark Riedi, Mauro Vareni, Maja Wüthrich, Mireia Marti, Marco Walser, wo contributed significantly during the sampling campaigns and sample processing. Large Language Models were only used to improve readability and style of the manuscript.

11 Financial support

The research was financially supported by the ExtremeThaw project as part of the WSL-funded Extremes program.

https://doi.org/10.5194/egusphere-2026-835
Preprint. Discussion started: 16 February 2026

12 References

Adamczyk, M., Hagedorn, F., Wipf, S., Donhauser, J., Vittoz, P., Rixen, C., Frossard, A., Theurillat, J. P., & Frey, B. (2019). The soil microbiome of Gloria Mountain summits in the Swiss Alps. *Frontiers in Microbiology*, *10*(MAY). https://doi.org/10.3389/fmicb.2019.01080

Agroscope. (2020). *Bestimmung des Gesamtkalkgehaltes (CaCO3) in Bodenproben* (Vol. 1). https://ira.agroscope.ch/de-CH/publication/45887

Baltensweiler, A., Heuvelink, G. B. M., Hanewinkel, M., & Walthert, L. (2020). Microtopography shapes soil pH in flysch regions across Switzerland. *Geoderma*, *380*(August), 114663. https://doi.org/10.1016/j.geoderma.2020.114663

Baltensweiler, A., Walthert, L., Ginzler, C., Sutter, F., Purves, R. S., & Hanewinkel, M. (2017). Environmental Modelling & Software Terrestrial laser scanning improves digital elevation models and topsoil pH modelling in regions with complex topography and dense vegetation. *Environmental Modelling and Software*, *95*, 13–21. https://doi.org/10.1016/j.envsoft.2017.05.009

Baltensweiler, A., Walthert, L., Hanewinkel, M., Zimmermann, S., & Nussbaum, M. (2021). Machine learning based soil maps for a wide range of soil properties for the forested area of Switzerland. *Geoderma Regional*, *27*(September), e00437. https://doi.org/10.1016/j.geodrs.2021.e00437

Baruck, J., Nestroy, O., Sartori, G., Baize, D., Traidl, R., Vrščaj, B., Bräm, E., Gruber, F. E., Heinrich, K., & Geitner, C. (2016). Soil classification and mapping in the Alps: The current state and future challenges. *Geoderma*, *264*, 312–331. https://doi.org/10.1016/j.geoderma.2015.08.005

Bayle, A., Gascoin, S., Corona, C., Stoffel, M., & Choler, P. (2025). Snow melt-out date (SMOD) change spanning four decades in European temperate mountains at 30 m from Landsat time series. *Scientific Data* , *12*(1), 1–11. https://doi.org/10.1038/s41597-025-05044-2

Bednorz, F., Reichstein, M., Broil, G., Holtmeier, F.-K., & Urfer, W. (2000). Humus Forms in the Forest-Alpine Tundra Ecotone at Stillberg (Dischmatal, Switzerland): Spatial Heterogeneity and Classification. *Arctic, Antarctic, and Alpine Research*, *32*(1), 21–29. https://doi.org/10.1080/15230430.2000.12003335

Behrens, T., Zhu, A. X., Schmidt, K., & Scholten, T. (2010). Multi-scale digital terrain analysis and feature selection for digital soil mapping. *Geoderma*, *155*(3–4), 175–185. https://doi.org/10.1016/j.geoderma.2009.07.010

Bockheim, J. G., & Munroe, J. S. (2014). Organic carbon pools and genesis of alpine soils with permafrost: A review. *Arctic, Antarctic, and Alpine Research*, *46*(4), 987–1006. https://doi.org/10.1657/1938-4246-46.4.987

Bolliger, J., Hagedorn, F., Leifeld, J., Böhl, J., Zimmermann, S., Soliva, R., & Kienast, F. (2008). Effects of land-use change on carbon stocks in Switzerland. *Ecosystems*, *11*(6), 895–907. https://doi.org/10.1007/s10021-008-9168-6

Bonfanti, N., Choler, P., Khedim, N., Clément, J. C., Barré, P., Goury, R., Baudin, F., Cécillon, L., Saillard, A., Thuiller, W., & Poulenard, J. (2025). Drivers of soil organic carbon stocks and stability along elevation gradients. *Geoderma*, *461*(August). https://doi.org/10.1016/j.geoderma.2025.117452

Bramble, D. S. E., Ulrich, S., Schöning, I., Mikutta, R., Brandt, L., Poll, C., Kandeler, E., Mikutta, C., Konrad, A., Siemens, J., Yang, Y., Polle, A., Schall, P., Ammer, C., Kaiser, K., & Schrumpf, M. (2024). Formation of mineral-associated organic

https://doi.org/10.5194/egusphere-2026-835
Preprint. Discussion started: 16 February 2026

matter in temperate soils is primarily controlled by mineral type and modified by land use and management intensity. *Global Change Biology*, *30*(1), 1–19. https://doi.org/10.1111/gcb.17024

Breiman, L. (2001). Random Forests. *Machine Learning*, *45*(1), 5–32. https://doi.org/10.1023/A:1010933404324

Bright, K., Dienes, B., Keiluweit, M., Rixen, C., & Aeppli, M. (2025). Climate change impacts on organic carbon cycling in European alpine soils. *Soil Biology and Biochemistry*, *210*(July), 109891. https://doi.org/10.1016/j.soilbio.2025.109891

Budge, K., Leifeld, J., Hiltbrunner, E., & Fuhrer, J. (2011). Alpine grassland soils contain large proportion of labile carbon but indicate long turnover times. *Biogeosciences*, *8*(7), 1911–1923. https://doi.org/10.5194/bg-8-1911-2011

Bui, E., Henderson, B., & Viergever, K. (2009). Using knowledge discovery with data mining from the Australian Soil Resource Information System database to inform soil carbon mapping in Australia. *Global Biogeochemical Cycles*, *23*(4), 1–15. https://doi.org/10.1029/2009GB003506

Chen, J., Elsgaard, L., Jan, K., Jørgen, V. G., Liang, Z., Jiang, Y., Lærke, P. E., Zhang, Y., Luo, Y., Hungate, B. A., Sinsabaugh, R. L., & Jørgensen, U. (2020). *Soil carbon loss with warming : New evidence from carbon-degrading enzymes*. *December 2019*, 1944–1952. https://doi.org/10.1111/gcb.14986

Chen, S., Wang, W., Xu, W., Wang, Y., Wan, H., Chen, D., Tang, Z., Tang, X., Zhou, G., Xie, Z., Zhou, D., Shangguan, Z., Huang, J., He, J. S., Wang, Y., Sheng, J., Tang, L., Li, X., Dong, M., … Bai, Y. (2018). Plant diversity enhances productivity and soil carbon storage. *Proceedings of the National Academy of Sciences of the United States of America*, *115*(16), 4027–4032. https://doi.org/10.1073/pnas.1700298114

Chen, Y., Qin, W., Zhang, Q., Wang, X., Feng, J., Han, M., Hou, Y., Zhao, H., Zhang, Z., He, J. S., Torn, M. S., & Zhu, B. (2024). Whole-soil warming leads to substantial soil carbon emission in an alpine grassland. *Nature Communications*, *15*(1). https://doi.org/10.1038/s41467-024-48736-w

Choler, P. (2015). Growth response of temperate mountain grasslands to inter-annual variations in snow cover duration. *Biogeosciences*, *12*(12), 3885–3897. https://doi.org/10.5194/bg-12-3885-2015

Choler, P., Bayle, A., Carlson, B. Z., Randin, C., Filippa, G., & Cremonese, E. (2021). The tempo of greening in the European Alps: Spatial variations on a common theme. *Global Change Biology*, *27*(21), 5614–5628. https://doi.org/10.1111/gcb.15820

Choler, P., Bayle, A., Fort, N., & Gascoin, S. (2024). *Waning snowfields have transformed into hotspots of greening within the alpine zone*. https://doi.org/10.1038/s41558-024-02177-x

Descombes, P., Walthert, L., Baltensweiler, A., Meuli, R. G., Karger, D. N., Ginzler, C., Zurell, D., & Zimmermann, N. E. (2020). Spatial modelling of ecological indicator values improves predictions of plant distributions in complex landscapes. *Ecography*, *43*(10), 1448–1463. https://doi.org/10.1111/ecog.05117

Egli, M., Mavris, C., Mirabella, A., & Giaccai, D. (2010). Soil organic matter formation along a chronosequence in the Morteratsch proglacial area (Upper Engadine, Switzerland). *Catena*, *82*(2), 61–69. https://doi.org/10.1016/j.catena.2010.05.001

Egli, M., Sartori, G., Mirabella, A., Favilli, F., Giaccai, D., & Delbos, E. (2009). Effect of north and south exposure on organic matter in high Alpine soils. *Geoderma*, *149*(1–2), 124–136. https://doi.org/10.1016/j.geoderma.2008.11.027

Fang, K., Qin, S., Chen, L., Zhang, Q., & Yang, Y. (2019). Al/Fe Mineral Controls on Soil Organic Carbon Stock Across Tibetan

https://doi.org/10.5194/egusphere-2026-835
Preprint. Discussion started: 16 February 2026

Alpine Grasslands. *Journal of Geophysical Research: Biogeosciences*, *124*(2), 247–259. https://doi.org/10.1029/2018JG004782

FOEN. (2025). *Switzerland's Greenhouse Gas Inventory 1990–2023: National Inventory Document and reporting tables (CRT). Submission of 2025 under the United Nations Framework Convention on Climate Change and under the Paris Agreement.* http://www.climatereporting.ch

Gavazov, K., Ingrisch, J., Hasibeder, R., Mills, R. T. E., Buttler, A., Gleixner, G., Pumpanen, J., & Bahn, M. (2017). Winter ecology of a subalpine grassland: Effects of snow removal on soil respiration, microbial structure and function. *Science of the Total Environment*, *590–591*, 316–324. https://doi.org/10.1016/j.scitotenv.2017.03.010

Georgiou, K., Angers, D., Champiny, R. E., Cotrufo, M. F., Craig, M. E., Doetterl, S., Grandy, A. S., Lavallee, J. M., Lin, Y., Lugato, E., Poeplau, C., Rocci, K. S., Schweizer, S. A., Six, J., & Wieder, W. R. (2025). Soil Carbon Saturation: What Do We Really Know? *Global Change Biology*, *31*(5), e70197. https://doi.org/https://doi.org/10.1111/gcb.70197

Gigon, A. (1987). *A Hierarchic Approach in Causal Ecosystem Analysis The Calcifuge-Calcicole Problem in Alpine Grasslands BT - Potentials and Limitations of Ecosystem Analysis* (E.-D. Schulze & H. Zwölfer (eds.); pp. 228–244). Springer Berlin Heidelberg. https://doi.org/10.1007/978-3-642-71630-0_11

Gomes, L. C., Faria, R. M., de Souza, E., Veloso, G. V., Schaefer, C. E. G. R., & Filho, E. I. F. (2019). Modelling and mapping soil organic carbon stocks in Brazil. *Geoderma*, *340*(December 2017), 337–350. https://doi.org/10.1016/j.geoderma.2019.01.007

Grabs, T., Seibert, J., Bishop, K., & Laudon, H. (2009). Modeling spatial patterns of saturated areas: A comparison of the topographic wetness index and a dynamic distributed model. *Journal of Hydrology*, *373*(1–2), 15–23. https://doi.org/10.1016/j.jhydrol.2009.03.031

Grêt-Regamey, A., & Weibel, B. (2020). Global assessment of mountain ecosystem services using earth observation data. *Ecosystem Services*, *46*. https://doi.org/10.1016/j.ecoser.2020.101213

Gubler, A., Wächter, D., & Schwab, P. (2018). Homogenisierung von Bodenkohlenstoff-Daten: Harmonisierung der Resultate aus Nassoxidation (FAL-Methode) und Trockenveraschung. *Agroscope Science*, *62*(62).

Guidi, C., Gosheva-oney, S., Didion, M., Flury, R., Walthert, L., Oney, B. J., Niklaus, P. A., Thürig, E., Viskari, T., & Liski, J. (2025). *Drivers of soil organic carbon from temperate to alpine forests : a model-based analysis of the Swiss forest soil inventory with Yasso20*. *December*, 1–26.

Gupta, S., Hasler, J. K., & Alewell, C. (2024). Mining soil data of Switzerland: New maps for soil texture, soil organic carbon, nitrogen, and phosphorus. *Geoderma Regional*, *36*(December 2023), e00747. https://doi.org/10.1016/j.geodrs.2023.e00747

Hagedorn, F., Gavazov, K., & Alexander, J. M. (2019). Above- and belowground linkages shape responses ofmountain vegetation to climate change. *Science*, *1123*(September), 1119–1123. https://doi.org/10.1126/science.aax4737

Hagedorn, F., Krause, H.-M., Studer, M., Schellenberger, A., & Gattinger, A. (2018). Boden und Umwelt - Organische Bodensubstanz, Treibhausgasemissionen und physikalische Belastung von Schweizer Böden. *Thematische Synthese TS2 Des Nationalen Forschungsprogramms «Nachhaltige Nutzung Der Ressource Boden»*, *NFP 68*.

Hagedorn, F., Mulder, J., & Jandl, R. (2010). Mountain soils under a changing climate and land-use. *Biogeochemistry*, *97*(1), 1–5.

https://doi.org/10.1007/s10533-009-9386-9

Hengl, T., Heuvelink, G. B. M., Kempen, B., Leenaars, J. G. B., Walsh, M. G., Shepherd, K. D., Sila, A., MacMillan, R. A., De Jesus, J. M., Tamene, L., & Tondoh, J. E. (2015). Mapping soil properties of Africa at 250 m resolution: Random forests significantly improve current predictions. *PLoS ONE*, *10*(6), 1–26. https://doi.org/10.1371/journal.pone.0125814

Hilinski, T. E. (2001). *Implementation of exponential depth distribution of organic carbon in the CENTURY model*. Department of Soil and Crop Science, Colorado State University.

Hoffmann, U., Hoffmann, T., Jurasinski, G., Glatzel, S., & Kuhn, N. J. (2014). Assessing the spatial variability of soil organic carbon stocks in an alpine setting (Grindelwald, Swiss Alps). *Geoderma*, *232–234*, 270–283. https://doi.org/10.1016/j.geoderma.2014.04.038

Hounkpatin, K., Stendahl, J., Lundblad, M., & Karltun, E. (2020). Predicting the spatial distribution of soil organic carbon stock in Swedish forests using remotely sensed and site-specific variables. *SOIL Discussions*, 1–30.

Hugelius, G., Strauss, J., Zubrzycki, S., Harden, J. W., Schuur, E. A. G., Ping, C. L., Schirrmeister, L., Grosse, G., Michaelson, G. J., Koven, C. D., O'Donnell, J. A., Elberling, B., Mishra, U., Camill, P., Yu, Z., Palmtag, J., & Kuhry, P. (2014). Estimated stocks of circumpolar permafrost carbon with quantified uncertainty ranges and identified data gaps. *Biogeosciences*, *11*(23), 6573–6593. https://doi.org/10.5194/bg-11-6573-2014

Hugelius, G., Tarnocai, C., Broll, G., Canadell, J. G., Kuhry, P., & Swanson, D. K. (2013). The northern circumpolar soil carbon database: Spatially distributed datasets of soil coverage and soil carbon storage in the northern permafrost regions. *Earth System Science Data*, *5*(1), 3–13. https://doi.org/10.5194/essd-5-3-2013

InfoFlora. (2024). *Jahresbericht / Rapport annuel / Rapporto annuale 2024*. https://www.infoflora.ch/de/home/news/2025/04/22/jahresbericht-2024/

Ioan, S., Roseo, F., & Brambilla, M. (2025). Mountain ecosystem services under a changing climate: A global perspective. *Ecosystem Services*, *73*(October 2024), 101732. https://doi.org/10.1016/j.ecoser.2025.101732

Iseli, E., Chisholm, C., Lenoir, J., Haider, S., Seipel, T., Barros, A., Hargreaves, A. L., Kardol, P., Lembrechts, J. J., McDougall, K., Rashid, I., Rumpf, S. B., Arévalo, J. R., Cavieres, L., Daehler, C., Dar, P. A., Endress, B., Jakobs, G., Jiménez, A., … Alexander, J. M. (2023). Rapid upwards spread of non-native plants in mountains across continents. *Nature Ecology and Evolution*, *7*(3), 405–413. https://doi.org/10.1038/s41559-022-01979-6

Jenny, H. (1946). *FACTORS OF SOIL FORMATION A System of Quantitative Pedology*. DOVER PUBLICATIONS, INC.

Jia, N., Li, L., Guo, H., & Xie, M. (2024). Important role of Fe oxides in global soil carbon stabilization and stocks. *Nature Communications* , *15*(1), 1–11. https://doi.org/10.1038/s41467-024-54832-8

Jobbágy, E. G., & Jackson, R. B. (2000). The vertical distribution of soil organic carbon and its relation to climate and vegetation. *Ecological Applications*, *10*(2), 423–436. https://doi.org/10.1890/1051-0761(2000)010[0423:TVDOSO]2.0.CO;2

Jones, D. L., Cooledge, E. C., Hoyle, F. C., Griffiths, R. I., & Murphy, D. V. (2019). pH and exchangeable aluminum are major regulators of microbial energy flow and carbon use efficiency in soil microbial communities. *Soil Biology and Biochemistry*, *138*(September), 0–4. https://doi.org/10.1016/j.soilbio.2019.107584

https://doi.org/10.5194/egusphere-2026-835
Preprint. Discussion started: 16 February 2026

Kuhn, M. (2008). Building predictive models in R using the caret package. *Journal of Statistical Software*, *28*(5), 1–26. https://doi.org/10.18637/jss.v028.i05

Kuhry, P., Makopoulou, E., Pascual Descarrega, D., Pecker Marcosig, I., & Trombotto Liaudat, D. (2022). Soil organic carbon stocks in the high mountain permafrost zone of the semi-arid Central Andes (Cordillera Frontal, Argentina). *Catena*, *217*(May), 106434. https://doi.org/10.1016/j.catena.2022.106434

Lamichhane, S., Kumar, L., & Wilson, B. (2019). Digital soil mapping algorithms and covariates for soil organic carbon mapping and their implications: A review. *Geoderma*, *352*(May), 395–413. https://doi.org/10.1016/j.geoderma.2019.05.031

Landolt, E., Bäumler, B., Ehrhardt, A., Hegg, O., Klötzli, F., Lämmler, W., Nobis, M., Rudmann-Maurer, K., Schweingruber, F., Theurillat, J.-P., Urmi, E., Vust, M., & Wohlgemuth, T. (2010). *Flora Indicativa – Ökologische Zeigerwerte und biologische Kennzeichen zur Flora der Schweiz und der Alpen*.

Lechler, L., Rixen, C., Bebi, P., Bavay, M., Marty, M., Barbeito, I., Dawes, M. A., Hagedorn, F., Krumm, F., Möhl, P., Schaub, M., & Frei, E. R. (2024). Five decades of ecological and meteorological data enhance the mechanistic understanding of global change impacts on the treeline ecotone in the European Alps. *Agricultural and Forest Meteorology*, *355*(June). https://doi.org/10.1016/j.agrformet.2024.110126

Leifeld, J., Bassin, S., & Fuhrer, J. (2005). Carbon stocks in Swiss agricultural soils predicted by land-use, soil characteristics, and altitude. *Agriculture, Ecosystems and Environment*, *105*(1–2), 255–266. https://doi.org/10.1016/j.agee.2004.03.006

Li, J., Heap, A. D., Potter, A., & Daniell, J. J. (2011). Application of machine learning methods to spatial interpolation of environmental variables. *Environmental Modelling and Software*, *26*(12), 1647–1659. https://doi.org/10.1016/j.envsoft.2011.07.004

Liu, S., Zhang, F., Du, Y., Guo, X., Lin, L., Li, Y., Li, Q., & Cao, G. (2016). Ecosystem carbon storage in alpine grassland on the Qinghai Plateau. *PLoS ONE*, *11*(8), 1–14. https://doi.org/10.1371/journal.pone.0160420

Maier, A., Macfarlane, M. E., Griepentrog, M., & Doetterl, S. (2025). Parent material geochemistry – and not plant input – as the primary element shaping soil organic carbon stocks in European alpine grasslands. *Biogeosciences*, *May*. http://dx.doi.org/10.5194/egusphere-2025-2006

Malik, A. A., Puissant, J., Buckeridge, K. M., Goodall, T., Jehmlich, N., Chowdhury, S., Gweon, H. S., Peyton, J. M., Mason, K. E., van Agtmaal, M., Blaud, A., Clark, I. M., Whitaker, J., Pywell, R. F., Ostle, N., Gleixner, G., & Griffiths, R. I. (2018). Land use driven change in soil pH affects microbial carbon cycling processes. *Nature Communications*, *9*(1), 1–10. https://doi.org/10.1038/s41467-018-05980-1

Martin, M. P., Wattenbach, M., Smith, P., Meersmans, J., Jolivet, C., Boulonne, L., & Arrouays, D. (2011). Spatial distribution of soil organic carbon stocks in France. *Biogeosciences*, *8*(5), 1053–1065. https://doi.org/10.5194/bg-8-1053-2011

Marty, C., Schlögl, S., Bavay, M., & Lehning, M. (2017). How much can we save? Impact of different emission scenarios on future snow cover in the Alps. *Cryosphere*, *11*(1), 517–529. https://doi.org/10.5194/tc-11-517-2017

McBratney, A. B., Mendonça Santos, M. L., & Minasny, B. (2003). On digital soil mapping. In *Geoderma* (Vol. 117, Issues 1–2). https://doi.org/10.1016/S0016-7061(03)00223-4

Meersmans, J., Van Wesemael, B., De Ridder, F., Dotti, M. F., De Baets, S., & Van Molle, M. (2009). Changes in organic carbon

https://doi.org/10.5194/egusphere-2026-835
Preprint. Discussion started: 16 February 2026

distribution with depth in agricultural soils in northern Belgium, 1960-2006. *Global Change Biology*, *15*(11), 2739–2750. https://doi.org/10.1111/j.1365-2486.2009.01855.x

Meinshausen, N. (2006). Quantile Regression Forests Nicolai. *Journal of Machine Learning Research*, *7*(6), 983–999. https://doi.org/10.1111/j.1541-0420.2010.01521.x

MeteoSchweiz. (2022). *Norm value charts*. RnormY9120 v2.0. https://www.meteoswiss.admin.ch/climate/the-climate-of-switzerland/climate-normals/norm-value-charts.html

MeteoSchweiz. (2024). *Normal values per measured parameter*. Climsheet 2.2.0. https://www.meteoswiss.admin.ch/climate/the-climate-of-switzerland/climate-normals/normal-values-per-measured-parameter.html

MeteoSwiss;, & ETH. (2025). *Climate CH2025 - Scientific Report*. https://doi.org/https://doi.org/10.18751/climate/scenarios/ch2025/sr/1.0/

Meuli, R. G., Wächter, D., Schwab, P., Kohli, L., & Zimmermann, R. (2017). Connecting Biodiversity Monitoring with Soil Inventory Data – A Swiss Case Study. *BGS Bulletin*, *38*, 65–69.

Meusburger, K., Trotsiuk, V., Schmidt-Walter, P., Baltensweiler, A., Brun, P., Bernhard, F., Gharun, M., Habel, R., Hagedorn, F., Köchli, R., Psomas, A., Puhlmann, H., Thimonier, A., Waldner, P., Zimmermann, S., & Walthert, L. (2022). Soil–plant interactions modulated water availability of Swiss forests during the 2015 and 2018 droughts. *Global Change Biology*, *April*, 5928–5944. https://doi.org/10.1111/gcb.16332

Meyer, H., & Pebesma, E. (2021). Predicting into unknown space? Estimating the area of applicability of spatial prediction models. *Methods in Ecology and Evolution*, *12*(9), 1620–1633. https://doi.org/https://doi.org/10.1111/2041-210X.13650

Minár, J., Evans, I. S., & Jenčo, M. (2020). A comprehensive system of definitions of land surface (topographic) curvatures, with implications for their application in geoscience modelling and prediction. *Earth-Science Reviews*, *211*(September 2019). https://doi.org/10.1016/j.earscirev.2020.103414

Minasny, B., & McBratney, A. B. (2016). Digital soil mapping: A brief history and some lessons. *Geoderma*, *264*, 301–311. https://doi.org/10.1016/j.geoderma.2015.07.017

Molnar, C., Casalicchio, G., & Bischl, B. (2018). iml: An R package for Interpretable Machine Learning. *Journal of Open Source Software*, *3*(26), 786. https://doi.org/10.21105/joss.00786

Musso, A., Lamorski, K., Sławiński, C., Geitner, C., Hunt, A., Greinwald, K., & Egli, M. (2019). Evolution of soil pores and their characteristics in a siliceous and calcareous proglacial area. *Catena*, *182*(May). https://doi.org/10.1016/j.catena.2019.104154

Naimi, B., Hamm, N. A. S., Groen, T. A., Skidmore, A. K., & Toxopeus, A. G. (2014). Where is positional uncertainty a problem for species distribution modelling? *Ecography*, *37*(2), 191–203. https://doi.org/10.1111/j.1600-0587.2013.00205.x

Nussbaum, M., & Burgos, S. (2021). *Soil Organic Carbon Stocks in Forests of Switzerland: Update of soil organic carbon stock estimation for the national greenhouse gas inventory*. *110012004*(August), 20.

Nussbaum, M., Papritz, A., Baltensweiler, A., & Walthert, L. (2014). *Estimating soil organic carbon stocks of Swiss forest soils by robust external-drift kriging*. *Cm*, 1197–1210. https://doi.org/10.5194/gmd-7-1197-2014

Pauli, H., Gottfried, M., Lamprecht, A., Niessner, S., Rumpf, S., Winkler, M., Steinbauer, K., & Grabherr, G. (2015). *The GLORIA*

https://doi.org/10.5194/egusphere-2026-835
Preprint. Discussion started: 16 February 2026

field manual – Standard multi-summit approach, supplementary methods and extra approaches – 5th edition. Publications Office. https://doi.org/doi/10.2777/867331

Peng, Z., Ma, T., Degen, A., Liu, P., Luo, B., Qi, L., Qi, T., Dengzeng, Z., Li, D., Wang, C., Lu, D., Qi, Y., Zheng, P., Guan, X., & Shang, Z. (2025). Plant detritus carbon dominates over microbial necromass carbon in topsoil of alpine ecosystems. *Communications Earth and Environment*, *6*(1), 1–9. https://doi.org/10.1038/s43247-025-02860-7

Pepin, N. C., Arnone, E., Gobiet, A., Haslinger, K., Kotlarski, S., Notarnicola, C., Palazzi, E., Seibert, P., Serafin, S., Schöner, W., Terzago, S., Thornton, J. M., Vuille, M., & Adler, C. (2022). Climate Changes and Their Elevational Patterns in the Mountains of the World. *Reviews of Geophysics*, *60*(1), 1–40. https://doi.org/10.1029/2020RG000730

Perez-Mon, C., Stierli, B., Plötze, M., & Frey, B. (2022). Fast and persistent responses of alpine permafrost microbial communities to in situ warming. *Science of the Total Environment*, *807*. https://doi.org/10.1016/j.scitotenv.2021.150720

Perruchoud, D., Walthert, L., Zimmermann, S., & Lüscher, P. (2000). Contemporary carbon stocks of mineral forest soils in the Swiss Alps. *Biogeochemistry*, *50*(2), 111–136. https://doi.org/10.1023/A:1006320129112

Ping, C. L., Michaelson, G. J., Jorgenson, M. T., Kimble, J. M., Epstein, H., Romanovsky, V. E., & Walker, D. A. (2008). High stocks of soil organic carbon in the North American Arctic region. *Nature Geoscience*, *1*(9), 615–619. https://doi.org/10.1038/ngeo284

Pintaldi, E., D'Amico, M. E., Colombo, N., Martinetto, E., Said-Pullicino, D., Giardino, M., & Freppaz, M. (2021). Hidden paleosols on a high-elevation Alpine plateau (NW Italy): Evidence for Lateglacial Nunatak? *Global and Planetary Change*, *207*(March). https://doi.org/10.1016/j.gloplacha.2021.103676

Poeplau, C., Vos, C., & Don, A. (2017). Soil organic carbon stocks are systematically overestimated by misuse of the parameters bulk density and rock fragment content. *Soil*, *3*(1), 61–66. https://doi.org/10.5194/soil-3-61-2017

Quan, Q., He, N., Zhang, R., Wang, J., Luo, Y., Ma, F., Pan, J., Wang, R., Liu, C., Zhang, J., Wang, Y., Song, B., Li, Z., Zhou, Q., Yu, G., & Niu, S. (2024). Plant height as an indicator for alpine carbon sequestration and ecosystem response to warming. *Nature Plants* , *10*(6), 890–900. https://doi.org/10.1038/s41477-024-01705-z

Reusser, J., Siegenthaler, M., Winkel, L., Wächter, D., Kretschmar, R., & Meuli, R. (2023). *Geochemischer Bodenatlas der Schweiz*. https://doi.org/10.34776/gca23-g

Rhyner, J., Bründl, M., Etter, H.-J., Steiniger, M., Stockli, D., Stucki, T., Zimmerli, M., & Ammann, W. (2002). *Avalanche Warning Switzerland – Consequences of the Avalanche Winter 1999*.

Richter, B., & Marty, C. (2026). Technical note: Literature based approach to estimate future snow. *Hydrology and Earth System Sciences*, *30*(3), 659–670. https://doi.org/10.5194/hess-30-659-2026

Rogiers, N., Hagedorn, F., & Thürig, E. (2025). *Forest Report 2025 - Development, Condition and Use of Swiss Forests*. https://doi.org/https://doi.org/10.55419/wsl:37786

Rowley, M. C., Grand, S., & Verrecchia, É. P. (2018). Calcium-mediated stabilisation of soil organic carbon. *Biogeochemistry*, *137*(1–2), 27–49. https://doi.org/10.1007/s10533-017-0410-1

Rumpf, S. B., Gravey, M., Brönnimann, O., Luoto, M., Cianfrani, C., Mariethoz, G., & Guisan, A. (2022). From white to green:

https://doi.org/10.5194/egusphere-2026-835
Preprint. Discussion started: 16 February 2026

Snow cover loss and increased vegetation productivity in the European Alps. *Science*, *1122*(June), 1119–1122. https://www.science.org

Shen, M., Wang, S., Jiang, N., Sun, J., Cao, R., Ling, X., Fang, B., Zhang, L., Zhang, L., Xu, X., Lv, W., Li, B., Sun, Q., Meng, F., Jiang, Y., Dorji, T., Fu, Y., Iler, A., Vitasse, Y., … Fu, B. (2022). Plant phenology changes and drivers on the Qinghai–Tibetan Plateau. *Nature Reviews Earth and Environment*, *3*(10), 633–651. https://doi.org/10.1038/s43017-022-00317-5

Siewert, M. B. (2018). High-resolution digital mapping of soil organic carbon in permafrost terrain using machine learning: A case study in a sub-Arctic peatland environment. *Biogeosciences*, *15*(6), 1663–1682. https://doi.org/10.5194/bg-15-1663-2018

Steinbauer, M. J., Grytnes, J.-A., Jurasinski, G., Kulonen, A., Lenoir, J., Pauli, H., Rixen, C., Winkler, M., Barni, M. B.-D. E., Bjorkman, A. D., Breiner, F. t., Burg, S., Czortek, P., Dawes, M. A., Delimat, A., Dullinger, S., Erschbamer, B., Felde, V. A., Fernández-Arberas, O., … Wipf, S. (2018). Accelerated increase in plant species richness on mountain summits is linked to warming. *Nature*, *556*, 231–234.

Streit, K., Hagedorn, F., Hiltbrunner, D., Portmann, M., Saurer, M., Buchmann, N., Wild, B., Richter, A., Wipf, S., & Siegwolf, R. T. W. (2014). Soil warming alters microbial substrate use in alpine soils. *Global Change Biology*, *20*(4), 1327–1338. https://doi.org/10.1111/gcb.12396

Stumpf, F., Behrens, T., Schmidt, K., & Keller, A. (2023). *Hinweiskarten für Bodeneigenschaften - Landesweit modellierte Karten für Bodeneigenschaften für drei Tiefenstufen* (Issue KOBO-Bericht Nr. 6).

Stumpf, F., Behrens, T., Schmidt, K., & Keller, A. (2024). Exploiting Soil and Remote Sensing Data Archives for 3D Mapping of Multiple Soil Properties at the Swiss National Scale. *Remote Sensing*, *16*(15). https://doi.org/10.3390/rs16152712

Stumpf, F., Keller, A., Schmidt, K., Mayr, A., Gubler, A., & Schaepman, M. (2018). Spatio-temporal land use dynamics and soil organic carbon in Swiss agroecosystems. *Agriculture, Ecosystems and Environment*, *258*(September 2017), 129–142. https://doi.org/10.1016/j.agee.2018.02.012

Swisstopo. (2024a). *DHM25 - The digital height model of Switzerland*. https://www.swisstopo.admin.ch/en/height-model-dhm25

Swisstopo. (2024b). *SwissTLM3D*. https://www.swisstopo.admin.ch/en/landscape-model-swisstlm3d

Swisstopo. (2025). *Objektkatalog swissTLM3D 2.3*. https://www.swisstopo.admin.ch/dam/de/sd-web/A3kQ2dAgenqG/2025-03 swissTLM3D 2.3 OK-DE.pdf

Trautmann, S., Knoflach, B., Stötter, J., Elsner, B., Illmer, P., & Geitner, C. (2023). Potential impacts of a changing cryosphere on soils of the European Alps: A review. *Catena*, *232*(February). https://doi.org/10.1016/j.catena.2023.107439

Udke, A., Marty, K., Bührer, C., Minich, L., Zehnder, M., Griepentog, M., Doetterl, S., Haghipour, N., Eglinton, T., Rixen, C., Egli, M., & Hagedorn, F. (2025). Non-linear increases of soil carbon stocks and turnover along alpine greening gradients on different bedrocks. *Submitted to Global Change Biology*.

Valavi, R., Elith, J., Lahoz-Monfort, J. J., & Guillera-Arroita, G. (2019). blockCV: An r package for generating spatially or environmentally separated folds for k-fold cross-validation of species distribution models. *Methods in Ecology and Evolution*, *10*(2), 225–232. https://doi.org/10.1111/2041-210X.13107

Vaysse, K., & Lagacherie, P. (2017). Using quantile regression forest to estimate uncertainty of digital soil mapping products.

https://doi.org/10.5194/egusphere-2026-835
Preprint. Discussion started: 16 February 2026

Geoderma, *291*, 55–64. https://doi.org/10.1016/j.geoderma.2016.12.017

Vitasse, Y., Ursenbacher, S., Klein, G., Bohnenstengel, T., Chittaro, Y., Delestrade, A., Monnerat, C., Rebetez, M., Rixen, C., Strebel, N., Schmidt, B. R., Wipf, S., Wohlgemuth, T., Yoccoz, N. G., & Lenoir, J. (2021). Phenological and elevational shifts of plants, animals and fungi under climate change in the European Alps. *Biological Reviews*, *96*(5), 1816–1835. https://doi.org/10.1111/brv.12727

Wadoux, A. M. J. C., & Heuvelink, G. B. M. (2023). Uncertainty of spatial averages and totals of natural resource maps. *Methods in Ecology and Evolution*, *14*(5), 1320–1332. https://doi.org/10.1111/2041-210X.14106

Wagner, J., Martin, V., Speetjens, N. J., A'Campo, W., Durstewitz, L., Lodi, R., Fritz, M., Tanski, G., Vonk, J. E., Richter, A., Bartsch, A., Lantuit, H., & Hugelius, G. (2023). High resolution mapping shows differences in soil carbon and nitrogen stocks in areas of varying landscape history in Canadian lowland tundra. *Geoderma*, *438*(August), 116652. https://doi.org/10.1016/j.geoderma.2023.116652

Walther, A. G., Beißner, S., & Burga, C. A. (2005). *Trends in the Upward Shift of Alpine Plants*. *16*(5), 541–548.

Walthert, L., Graf, U., Kammer, A., Luster, J., Pezzotta, D., Zimmermann, S., & Hagedorn, F. (2010). Determination of organic and inorganic carbon, δ13C, and nitrogen in soils containing carbonates after acid fumigation with HCl. *Journal of Plant Nutrition and Soil Science*, *173*(2), 207–216. https://doi.org/10.1002/jpln.200900158

Wang, C., & Kuzyakov, Y. (2024). Soil organic matter priming: The pH effects. *Global Change Biology*, *30*(6), 1–21. https://doi.org/10.1111/gcb.17349

Wiesmeier, M., Barthold, F., Spörlein, P., Geuß, U., Hangen, E., Reischl, A., Schilling, B., Angst, G., Von Lützow, M., & Kögel-Knabner, I. (2014). Estimation of total organic carbon storage and its driving factors in soils of Bavaria (southeast Germany). *Geoderma Regional*, *1*(C), 67–78. https://doi.org/10.1016/j.geodrs.2014.09.001

Wiesmeier, M., Urbanski, L., Hobley, E., Lang, B., von Lützow, M., Marin-Spiotta, E., van Wesemael, B., Rabot, E., Ließ, M., Garcia-Franco, N., Wollschläger, U., Vogel, H. J., & Kögel-Knabner, I. (2019). Soil organic carbon storage as a key function of soils - A review of drivers and indicators at various scales. *Geoderma*, *333*(July 2018), 149–162. https://doi.org/10.1016/j.geoderma.2018.07.026

Wright, M. N., & Ziegler, A. (2017). Ranger: A fast implementation of random forests for high dimensional data in C++ and R. *Journal of Statistical Software*, *77*(1). https://doi.org/10.18637/jss.v077.i01

Yang, R., Rossiter, D. G., Liu, F., Lu, Y., Yang, F., Yang, F., Zhao, Y., Li, D., & Zhang, G. (2015). Predictive mapping of topsoil organic Carbon in an Alpine environment aided by Landsat TM. *PLoS ONE*, *10*(10), 1–20. https://doi.org/10.1371/journal.pone.0139042

Yang, Y., Fang, J., Tang, Y., Ji, C., Zheng, C., He, J., & Zhu, B. (2008). Storage, patterns and controls of soil organic carbon in the Tibetan grasslands. *Global Change Biology*, *14*(7), 1592–1599. https://doi.org/10.1111/j.1365-2486.2008.01591.x

Zehnder, M., Pfund, B., Svoboda, J., Marty, C., Vitasse, Y., Alexander, J., Hille Ris Lambers, J., & Rixen, C. (2025). Snow Height Sensors Reveal Phenological Advance in Alpine Grasslands. *Global Change Biology*, *31*(5). https://doi.org/10.1111/gcb.70195

Zhang, G., & Lu, Y. (2012). Bias-corrected random forests in regression. *Journal of Applied Statistics*, *39*(1), 151–160.

https://doi.org/10.5194/egusphere-2026-835
Preprint. Discussion started: 16 February 2026

https://doi.org/10.1080/02664763.2011.578621

Zhang, M., Zhou, A., Cao, S., Yuan, Y., & Han, N. (2025). Multi-angle study on carbon stock variation and its driving factors in Pingshan County. *Scientific Reports*, *15*(1), 1–19. https://doi.org/10.1038/s41598-025-91610-y

Zhang, Y., Chen, A., Wang, Z., Wang, X., Lin, Y., & Ye, C. (2023). Catena Soil organic carbon accumulation along a chronosequence of vegetation colonization on debris flow fans in Southwest China. *Catena*, *223*(June 2022), 106936. https://doi.org/10.1016/j.catena.2023.106936

Zilker, F., & Karger, D. N. (2025). *CHELSAch-highres-climatologies at high resolution*. EnviDat. https://doi.org/10.16904/envidat.689

https://doi.org/10.5194/egusphere-2026-835
Preprint. Discussion started: 16 February 2026

A. Appendix A): Modelling and environmental variables

Table A1: Description and sources of spatial covariates in final QRF model and their expected effects on SOC stocks.

	Variable	Resolution	Source	Description and expected influence on SOC
A priori	Landolt-H (-)	90 m	Descombes et al. (2020)	Represents Landolt humus value (Landolt et al., 2010) averaged from georeferenced species records. It is a proxy for topsoil humus content. Landolt-H shows a positive correlation with SOC as it was empirically assessed based on humus preference of a given plant species.
	Landolt-R (-)	90 m	Descombes et al. (2020)	Represents Landolt reaction value (Landolt et al., 2010) averaged from georeferenced species records. It is a proxy for topsoil pH. Higher Landolt-R values (higher pH, calcareous bedrock) are associated with lower SOC stocks due to shallow soils and limited formation of reactive mineral surfaces for SOC stabilization (Wiesmeier et al, 2019, Trautmann et al., 2024, Rowley et al., 2018)
	NDVI (-)	25 m	Sentinel-2, Google Earth Engine (Copernicus/S2_SR)	Normalized Difference Vegetation Index (NDVI) represents vegetation greenness; derived from Sentinel-2 bottom-of-atmosphere scenes and aggregated into a median (June – August) for 2015–2018. In alpine regions, higher NDVI is associated with higher SOC stocks via greater C inputs.
	Temperature (°C)	90 m	Zilker & Karger (2025)	Mean summer air temperature (CHELSA) averaged across the months of June – August using the source data. In alpine environments, higher temperatures support increased decomposition and leading to higher SOC stocks (Bonfanti et al., 2025; Trautmann et al., 2024).
	Precipitation (mm day^{-1})	90 m	Zilker & Karger (2025)	Precipitation represents the average daily precipitation, averaged across all months from source data. Higher precipitation increases SOC stocks by promoting biomass production and limiting decomposition (Jobbágy & Jackson, 2000).
	Melt-out day (DOY)	25 m	Bayle et al. (2025)	Average annual melt-out day of year (DOY) between 2012 and 2022 calculated above 1750 m using source. Earlier melt-out is associated with longer growing seasons and increased biomass production (Choler, 2015), favouring SOC accumulation in alpine soils.
Multiscale approach (Table A2)	Northness (-)	25 m	Derived from DEM (Swisstopo, 2024a)	Cosine of the aspect, which affects potential solar radiation, primary production, evapotranspiration and soil temperatures. Higher values indicate more north-facing slopes. SOC stocks are higher on north-facing slopes due to lower temperature limiting decomposition.
	Slope (rad)	25 m	Derived from DEM, (Baltensweiler et al., 2020)	The average local slope steepness, capturing erosion potential. Steeper slopes are associated with lower SOC stocks due to enhanced erosion, and faster drainage, which limit SOC accumulation.
	Curvature (-)	25 m	Calculated from DEM, (Baltensweiler et al., 2017)	Casorati curvature, derived from the DEM. It is a measure of the magnitude of surface bending, calculated after smoothing with an 8-pixel kernel. SOC stocks decrease with high casorati-curvature because of limitted organic matter retention or surface instability and soil erosion on sharp ridges or in steep depressions.
	TWI (-)	25 m	Calculated from DEM, (Baltensweiler et al., 2017)	SAGA TWI, smoothed with an 8-pixel kernel, integrates local slope and upslope contributing area to approximate the potential for soil moisture accumulation and drainage. Higher values indicate concave positions with greater water convergence and reduced drainage. Higher TWI is associated with higher SOC stocks due to sustained soil moisture and material accumulation (Grabs et al., 2009).

https://doi.org/10.5194/egusphere-2026-835
Preprint. Discussion started: 16 February 2026

Choice of topographic covariable data: Multiscale approach

To identify the most informative topographic predictors for SOC modelling, we tested a comprehensive set of variables derived from the DEM of Switzerland at 25m resolution (Swisstopo, 2024a). These included multiple representations of local and regional terrain attributes at different scales (Baltensweiler et al., 2017, 2020). First, highly correlated variables (cutoff = 0.95) and topographic predictors characterized by highly localized extreme values (e.g. extreme flow-path metrics) were removed, resulting in a set of 46 topographic candidate predictors (Table A2). To reduce conceptual redundancy, the remaining 46 topographic predictors were grouped into four distinct feature types, which are known to have an effect on SOC accumulation and storage:

- Regional terrain (TWI, TPI, mean upslope gradient; capturing landscape position and regional moisture accumulation potential)
- Local curvature (including plan, profile, tangential, and Casorati curvature; capturing local surface geometry)
- Slope-related attributes (e.g. slope steepness, capturing local erosion potential)
- Aspect-related attributes (aspect and potential solar radiation, capturing topographically driven differences in energy balance and microclimate)

These 46 topographic variables were evaluated within a QRF *together* with the a-priori selected covariables using spatial cross-validation (Valavi et al., 2019). Within each topographic feature type, the highest-ranking predictor based on node impurity was selected for the final model. Selected was the SAGA-derived TWI with and 8-cell smoothing (TWI_SAGA_s8_25m), Casorati curvature (curv_casorati_25m_s8), northness, and the local slope in radians (slpM0_25m). The selected topographic variables are described in detail together with a-priori selected environmental variables in Table A1.

The QRF model used for selecting topographic variables showed slightly lower performance (R^2 = 0.47; RMSE = 2.74) than the final model based on the reduced, selected predictor set.

https://doi.org/10.5194/egusphere-2026-835
Preprint. Discussion started: 16 February 2026

Table A2: Relative variable importance of a-priori selected and topographic predictors in the QRF model. Predictors are grouped by conceptual topographic feature type. Highest ranking variables within a topographic feature type, which were selected for further modelling, are printed in bold. Shown are only the 10 highest ranking predictors per feature type. Variable abbreviations represent different smoothings (s) and various parametrizations and methods, which are described in detail in Baltensweiler et al. (2017) and Baltensweiler et al. (2020). Note that for variables with an apparently reduced number of parametrizations, alternative parametrizations were removed during the multicollinearity filtering step.

Variable	Importance	Feature type
NDVI	100.00	A priori
Landolt-H	85.60	
Temperature	23.20	
Landolt-R	11.70	
Meltout	6.28	
Precipitation	4.73	
TWI_SAGA_s8_25m	5.29	Regional terrain
catchSlpM0_s4_25m	2.51	
TWI_M0top_s2_25m	2.08	
TWI_M1_s2_25m	2.07	
TWI_M1top_25m	2.04	
TWI_SAGA_modArea_s8_25m	1.93	
catchSlpM0_25m	1.93	
TWI_M0top_25m	1.91	
tpi2000c_25m	1.35	
catchSlpM1_25m	1.25	
curv_casorati_25m_s8	3.67	Local curvature
curv_tan_25m_s2	2.02	
curv_plan_25m_s4	1.77	
curv_contour_25m_s4	1.72	
curv_tan_25m_s8	1.45	
curv_casorati_25m_s4	1.38	
convexity_3_25m	1.24	
curv_plan_25m_s8	1.15	
curv_profile_25m_s4	1.12	
curv_tan_25m_s4	1.06	
northness_25m	8.81	Aspect
Solar radiation	5.42	
eastness_25m	1.43	
slpM0_25m	0.96	Slope
slpM6_25m	0.66	

https://doi.org/10.5194/egusphere-2026-835
Preprint. Discussion started: 16 February 2026

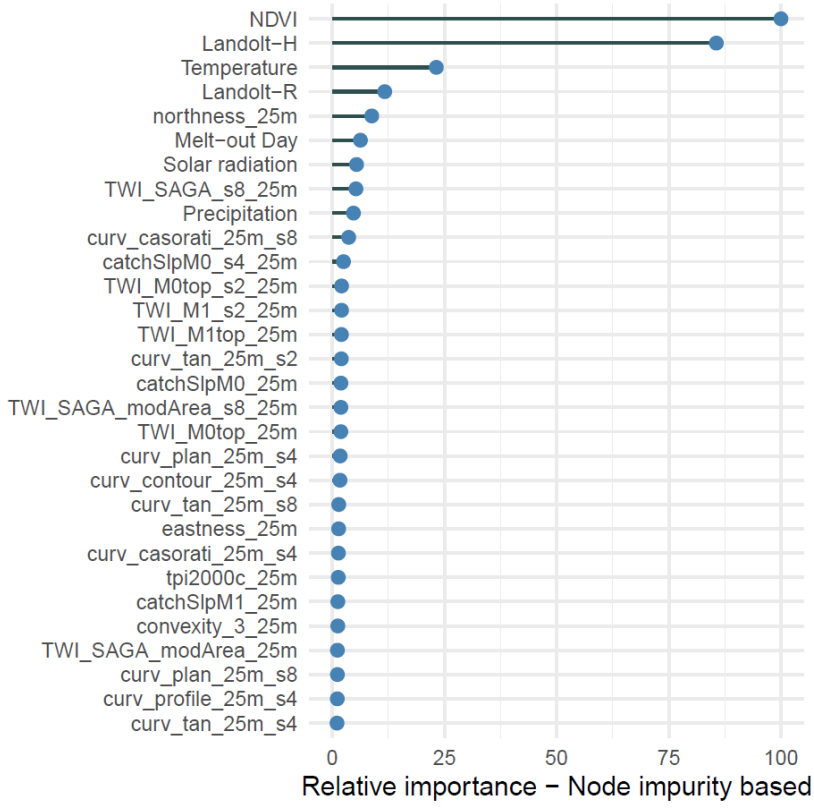

Figure A1: Relative variable importance for topography-related covariables derived from the DEM tested together with the a priori selected covariables (ranking highest). Only the 30 highest ranking variables are shown. Abbreviations of topographic variables are corresponding to Baltensweiler et al. (2017) and Baltensweiler et al. (2020).

https://doi.org/10.5194/egusphere-2026-835
Preprint. Discussion started: 16 February 2026

Spatial cross-validation and hyperparameter tuning of final QRF model

Across all tested combinations of hyperparameters in the spatial cross-validation QRF (Figure A2), mtry = 7, and min.node.size = 7 resulted in the optimal QRF model with an RMSE of 2.71 and an R^2 of 0.49 (Figure A3). Differently sized grid sizes for fold assignment did not significantly affect the model performance. The splitrule of extremely randomized trees (extra-trees) lead to significantly lower RMSE than "splitrule = variance". These hyperparameters were then used in the final predictive QRF trained with all data. The full model trained on all observations showed high in-sample performance, with an RMSE of 1.56 kg m^{-2} and an R^2 of 0.83.

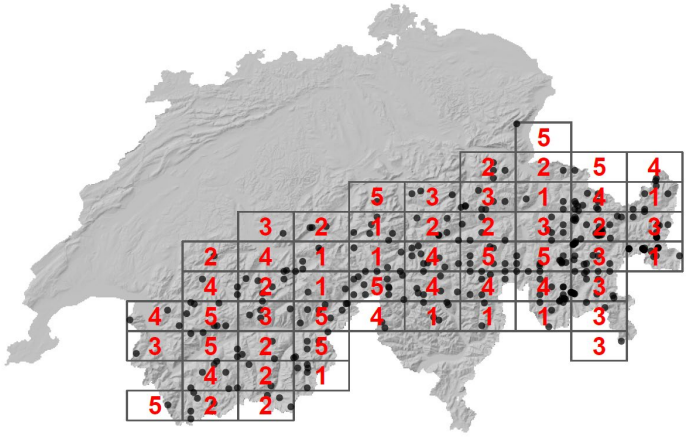

Figure A2: Spatial cross-validation grid used for model training and validation using the R-package blockCV (Valavi et al., 2019). Numbers show the fold assignments (1–5) within each spatial block used to create spatially independent training and testing subsets. Geographically close samples are assigned to the same fold, thereby minimizing spatial autocorrelation between training and validation data. Differently sized grid sizes did not significantly affect the model performance.

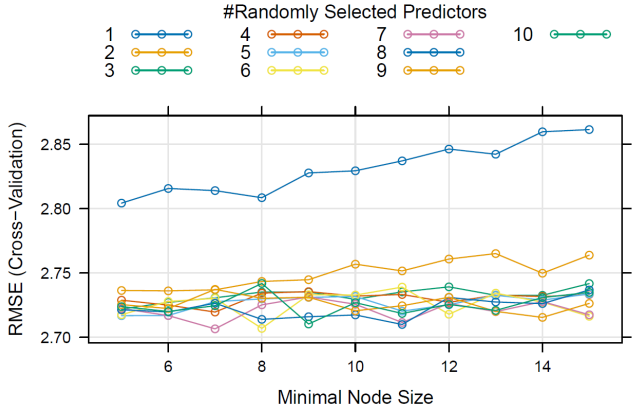

Figure A3: Cross-validation results of the QRF model showing the relationship between the number of randomly selected predictors (mtry), minimal node size and model performance (RMSE). Lines represent different values of the mtry. Lower RMSE values indicate better predictive performance, with the smallest node size of 7 and mtry of 7 yielding the overall lowest cross-validation error. Results are shown for extremely randomized trees (extra-trees), which lead to significantly lower RMSE than "splitrule = variance" (results not shown).

https://doi.org/10.5194/egusphere-2026-835
Preprint. Discussion started: 16 February 2026

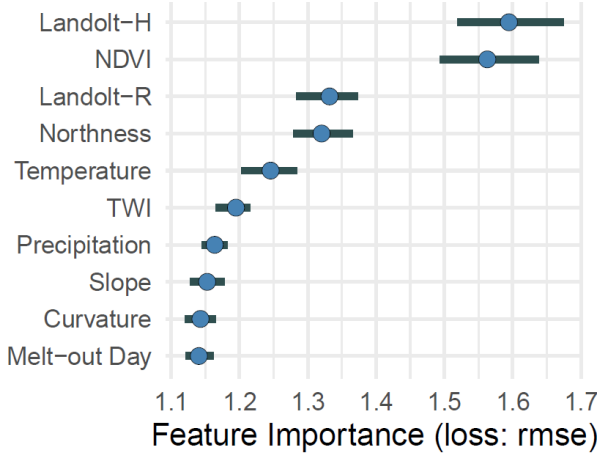

Figure A4: Feature importance of spatial CV QRF based on feature permutation (Molnar et al, 2018). Shown is the increase in RMSE when each covariate is randomly permuted, indicating its relative contribution to model accuracy. A higher RMSE loss means greater importance of the variable for predicting SOC stocks. Notably, Landolt-R and northness ranked higher under permutation-based importance than under node-impurity-based importance (Figure 5). Melt-out day, precipitation and curvature contributed less to model accuracy.

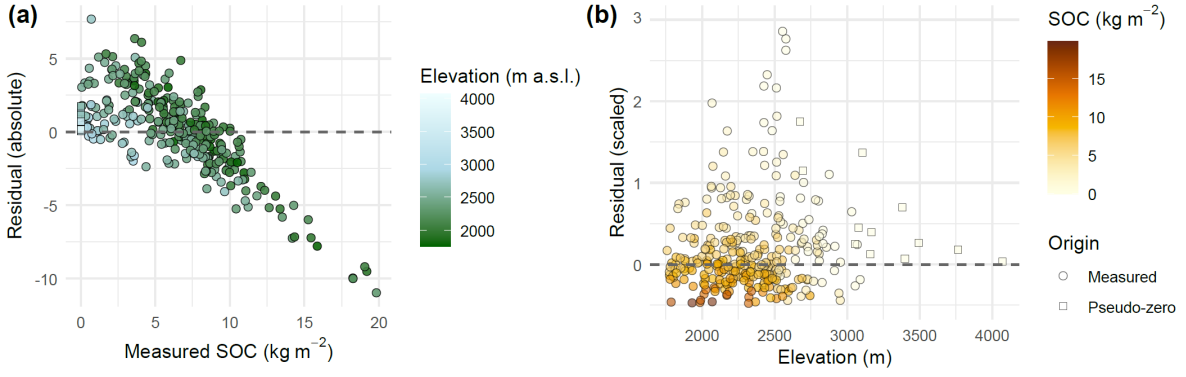

Figure A5: Model residuals (predicted – observed SOC stocks in kg m^{-2}) from spatial cross-validation of a QRF model predicting SOC stocks. a) Residuals plotted against observed SOC values, with points coloured by residual magnitude (positive residual = overestimation, negative residual = underestimation), showing expected regression towards the mean: sites with low stocks show an overestimation, while sites with high stocks show an underestimation. b) Scaled residuals of SOC stock predictions plotted against elevation. Scaled residuals were calculated as (Predicted−Observed)/(Observed+1). Points are coloured by measured SOC stocks (light to dark brown). There is no systematic bias across elevation, whereby some sites at mid-elevation show the highest model error.

https://doi.org/10.5194/egusphere-2026-835
Preprint. Discussion started: 16 February 2026

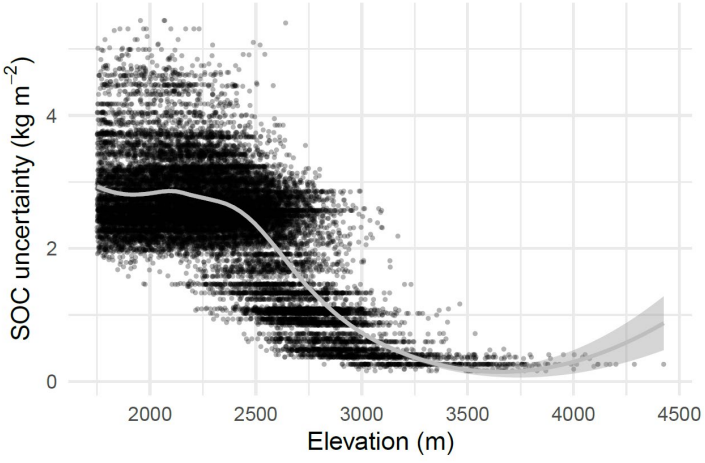

Figure A6: Relationship between elevation and model uncertainty (standard error) of SOC predictions derived from the QRF model. Each point represents a random sample of pixels from the uncertainty map (n_random = 20'000). The sometimes-discrete horizontal banding reflects the quantilized nature of QRF-derived uncertainty values, which result from discrete output levels in the predicted median quantiles where each terminal node stores only the training observations that fell into it.

https://doi.org/10.5194/egusphere-2026-835
Preprint. Discussion started: 16 February 2026

Table A3: Summary statistics of SOC stocks and environmental predictor variables used in the QRF model. Additionally, the summary statistics for "elevation" based on the DEM were added for each cover class. Note that Landolt-H is translated to pH-scale (Descombes et al., 2021).

Cover class	Variable	mean	median	sd	min	max
Grassland (n= 259)	SOC (kg m⁻²)	7.28	7.22	3.27	0.70	19.83
	Landolt-R (–)	5.80	5.80	0.35	5.13	6.78
	Landolt-H (–)	3.29	3.30	0.26	2.40	4.01
	NDVI (–)	0.57	0.59	0.13	0.19	0.80
	Melt-out day (DOY)	147.2	151	19.3	86	203
	Precipitation (mm month⁻¹)	3.73	3.37	1.48	1.50	9.70
	Temperature (°C)	7.70	7.68	1.39	4.54	11.25
	Northness (–)	-0.18	-0.31	0.66	-1.00	1.00
	TWI (–)	3.69	3.67	0.67	2.15	5.66
	Casorati curvature (–)	0.47	0.45	0.19	0.07	1.19
	slpM0_25m	0.35	0.33	0.20	0.00	1.11
	Elevation (m a.s.l)	2,250	2,244	242	1,759	2,794
(Vegetated) Scree (n=37)	SOC (kg m⁻²)	1.80	1.32	1.67	0.07	8.46
	Landolt-R (–)	6.06	6.25	0.55	5.20	6.88
	Landolt-H (–)	2.53	2.56	0.31	1.91	3.09
	NDVI (–)	0.16	0.14	0.10	0.01	0.41
	Melt-out day (DOY)	172.9	172	17.6	139	213
	Precipitation (mm month⁻¹)	2.85	2.51	1.01	1.94	6.15
	Temperature (°C)	5.10	4.84	1.22	1.67	7.17
	Northness (–)	0.00	0.13	0.75	-1.00	1.00
	TWI (–)	3.21	3.00	0.71	2.17	5.30
	Casorati curvature (–)	0.65	0.71	0.23	0.28	1.05
	slpM0_25m	0.35	0.34	0.21	0.04	0.84
	Elevation (m a.s.l)	2,703	2,716	188	2,265	3,069
Exposed Rock (n=11)	SOC (kg m⁻²)	1.17	0.57	1.42	0.09	4.80
	Landolt-R (–)	5.73	5.56	0.45	5.19	6.43
	Landolt-H (–)	2.55	2.41	0.31	2.15	3.05
	NDVI (–)	0.09	0.08	0.10	-0.03	0.26
	Melt-out day (DOY)	176.3	175	8.4	163	193
	Precipitation (mm month⁻¹)	3.50	3.21	1.39	2.06	6.34
	Temperature (°C)	4.47	4.67	1.63	1.41	7.45
	Northness (–)	0.17	0.32	0.71	-0.96	0.98
	TWI (–)	3.33	3.24	0.89	2.22	4.86
	Casorati curvature (–)	0.73	0.82	0.24	0.38	1.04
	slpM0_25m	0.46	0.42	0.30	0.11	0.99
	Elevation (m a.s.l)	2,762	2,802	218	2,392	3,089

https://doi.org/10.5194/egusphere-2026-835
Preprint. Discussion started: 16 February 2026

Bivariate relationships between spatial covariates and SOC stocks

The bivariate linear relationships shown below are intended as an exploratory illustration of the general relationships between SOC stocks and individual covariables. They are not directly relevant for the QRF model, which captures non-linear effects and interactions among multiple predictors simultaneously and does not rely on linear assumptions.

Bivariate linear regressions showed clear relationships between SOC stocks and environmental predictors (FigureS13). SOC stocks increased with higher NDVI and greater Landolt-H values, indicating higher C stocks in more productive and humus-rich plant communities, with Landolt-H explaining the largest share of variance among all predictors. SOC also increased with higher temperatures. In contrast, later melt-out dates were associated with lower SOC stocks, consistent with shorter growing seasons and reduced annual C inputs under prolonged snow cover. Topographic variables exerted weaker relationship: SOC tended to be lower on roughly curved terrain (indicating mountain ridges and summits) and showed only a minor dependence on northness. TWI showed a positive relationship, hinting at higher SOC stocks in depressions and areas where water can accumulate. Landolt-R exhibited a weak negative relationship with SOC, in line with reduced C storage on calcareous substrates with less reactive mineral surfaces.

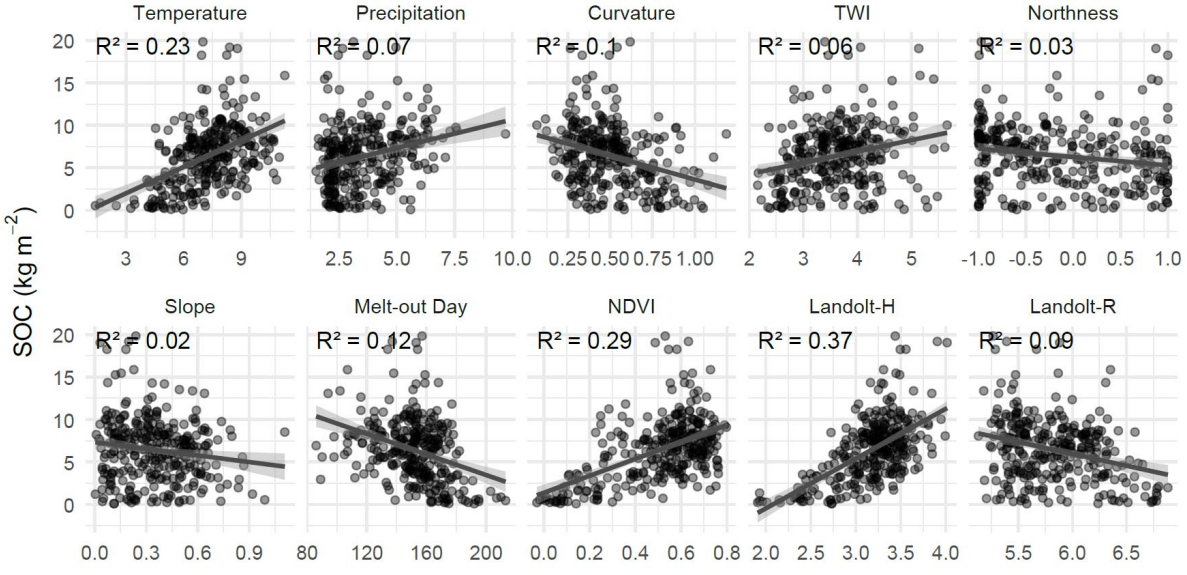

Figure A7: Bivariate relationships between SOC stocks and all environmental predictors used in the QRF model. Each panel shows a simple linear fit with coefficient of determination (R^2) indicating the strength of association based on linear fits. Units can be found in Table A3 above.

https://doi.org/10.5194/egusphere-2026-835
Preprint. Discussion started: 16 February 2026

Elevational decline of SOC stocks, NDVI threshold and relationship between productivity and aspect

SOC stocks declined relatively sharply at around 2600 m a.s.l., coinciding with the upper limit of continuous vegetation cover and a marked reduction in litter inputs to the soil. Soil profiles along elevation gradients used to constrain PTF showed the same pattern (Udke et al., submitted). The sigmoidal model explained slightly more variance in SOC stocks along the elevational gradient (pseudo-R^2 = 0.29) than a linear model (R^2 = 0.24).

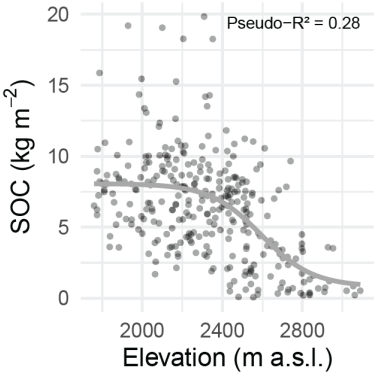

Figure A8. Relationship between elevation and SOC stocks across all sites (n=307). Points represent individual observations, and the solid line shows a fitted sigmoidal curve highlighting the nonlinear decline in SOC stocks with increasing elevation.

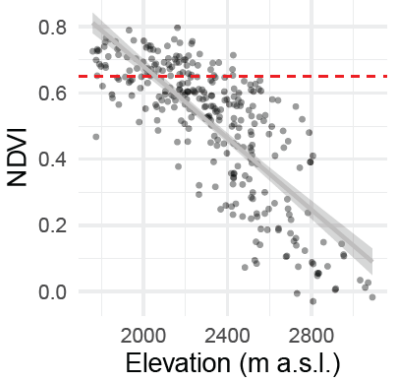

Figure A9: Relationship between elevation and vegetation greenness/productivity expressed as the Normalized Difference Vegetation Index (NDVI). Points represent individual observation sites, and the red dashed horizontal line indicates an NDVI value of 0.65, corresponding to dense alpine grassland vegetation where the effect of NDVI on SOC stocks begins to saturate according to partial dependence analyses of the QRF (Figure 6). The smooth illustrates the general linear elevational trend in NDVI.

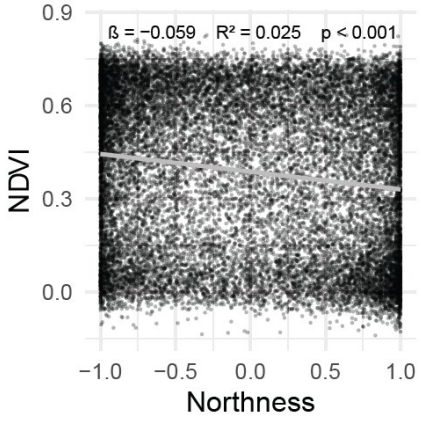

Figure A10: Shown are pixel-wise comparisons of 20,000 randomly sampled pixels from the NDVI and northness layers. Northness is defined as the cosine of aspect, with higher values indicating north-facing slopes. NDVI decreases with increasing northness (β = −0.059, R^2 = 0.025, $p < 0.001$), indicating higher vegetation productivity on south-facing slopes in the Alpine regions of Switzerland.

https://doi.org/10.5194/egusphere-2026-835
Preprint. Discussion started: 16 February 2026

B. Appendix B): Pedotransfer functions (PTF)

Profile data to constrain PTF functions

Profile data from 17 soil pits reaching bedrock (Figure B1) was examined in-depth and published in Udke et al. *(submitted)*. Here, we used the three variables required to calculate SOC stocks; $SOC_{\%}$ (i.e. the percentage content of organic C in homogenized FE), FE density, and coarse rock fraction (i.e. the percentage of the coarse rock fraction >2 mm in the sampled volume) (Poeplau et al., 2017). These three parameters were derived from environmentally matching soil profile data to constrain PTF to model subsoil SOC stocks of all sites with the procedure explained after the description of each parameter measured at profile sites. Profiles on silicious bedrock used in the PTF are located between 2000 - 3040 m a.s.l. and are placed along two transects while profiles on calcareous bedrock are located between 2000 - 2800 m and were sampled along one transect.

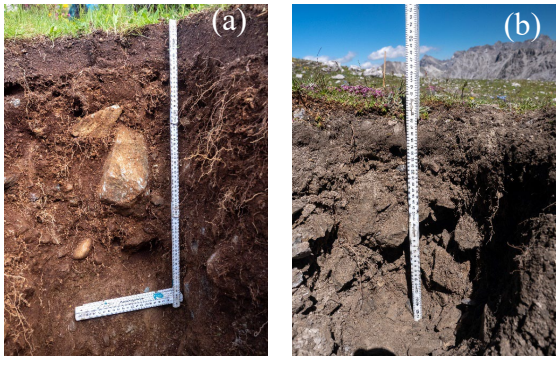

Figure B1: Exemplar soil profiles on (a) gneissic bedrock, 2175 m a.s.l. and (b) calcareous bedrock, 2750 m a.s.l., which were excavated along elevational gradients. The soil properties of these sites were used to parametrize PTF to extrapolate SOC stocks from topsoil sampling sites to deeper soil layers below 20 cm.

https://doi.org/10.5194/egusphere-2026-835
Preprint. Discussion started: 16 February 2026

Soil organic carbon concentration ($SOC_{\%}$) at profile sites

$SOC_{\%}$ declined systematically with increasing soil depth across all sites (Figure B2). Unsurprisingly, surface horizons consistently exhibited the highest $SOC_{\%}$ and followed an exponential decrease with soil depth. This exponential decay is commonly implemented in soil-depth models of $SOC_{\%}$ (Hilinski, 2001; Meersmans et al., 2009). The intercept and exponential decline rate varied among sites. As was to be expected, sites at lower elevation showed higher $SOC_{\%}$.

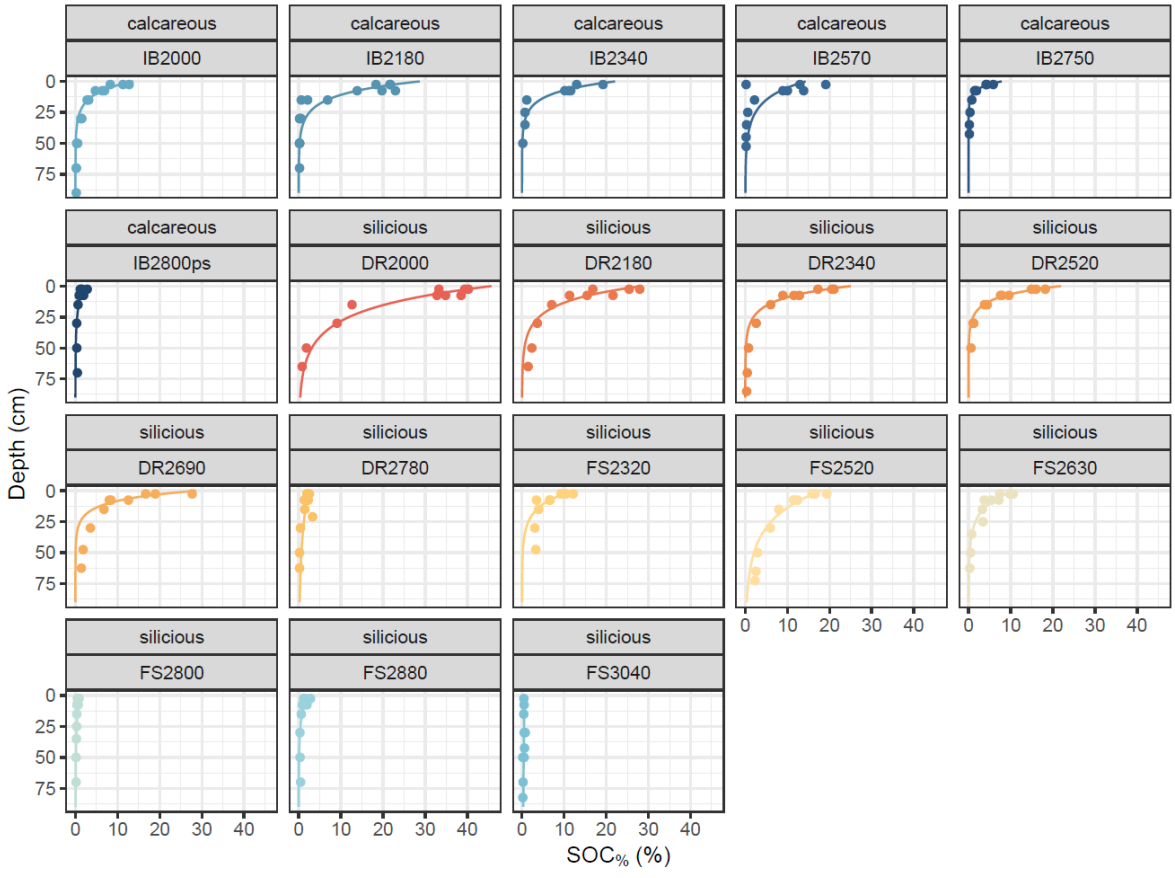

Figure B2: Depth profiles of $SOC_{\%}$ for profile sites used to constrain PTF. Panels are grouped by bedrock type (calcareous vs. siliceous) and colored by sites. Points show measured $SOC_{\%}$ values at each sampling depth, and the fitted exponential relationship with depth. Note that elevation is indicated by the four-digit site identifiers (e.g., IB2180; 2180 m a.s.l.) while the letters stand for the transect ID.

Note that, although an attempt was made to excavate a full soil profile at 2800 m on calcareous bedrock, extremely rocky ground prevented sampling beyond 5 cm. This site (IB2800) was therefore excluded from the PTF modelling workflow. Without this profile, the next-highest calcareous site (IB2750) would disproportionately influence the selection of suitable high-elevation reference profiles. Moreover, the highest complete calcareous profile available (IB2750) represents an unusually densely vegetated site (vegetation cover > 75 %) and exhibits comparatively high $SOC_{\%}$. To avoid systematic overestimation of modelled subsoil SOC for calcareous bedrock at high elevation, we generated a pseudoprofile (IB2800ps) by duplicating the depth trajectory of DR2800 (a siliceous site), thereby providing a more conservative and representative upper-elevation reference profile for this parent material.

https://doi.org/10.5194/egusphere-2026-835
Preprint. Discussion started: 16 February 2026

Fine earth (FE) density

Fine earth density showed a linear relationship with depth (Figure B3), although in some cases (DR2520, DR2340; both on silicious bedrock in a similar elevational range) an exponential function also showed good fits (results not shown). Fitting exponential functions, however, would lead to overestimations of SOC stocks in the subsoil and therefore linear fits were used. FE density increased with depth at most sites, in some cases exceeding 2 g cm^{-3} at greater depths. Across the sites, the intercept at the surface and slope of the FE density values vary, allowing us to choose the best fit for each topsoil site depending on the depth trajectory of FE density measured at each topsoil site.

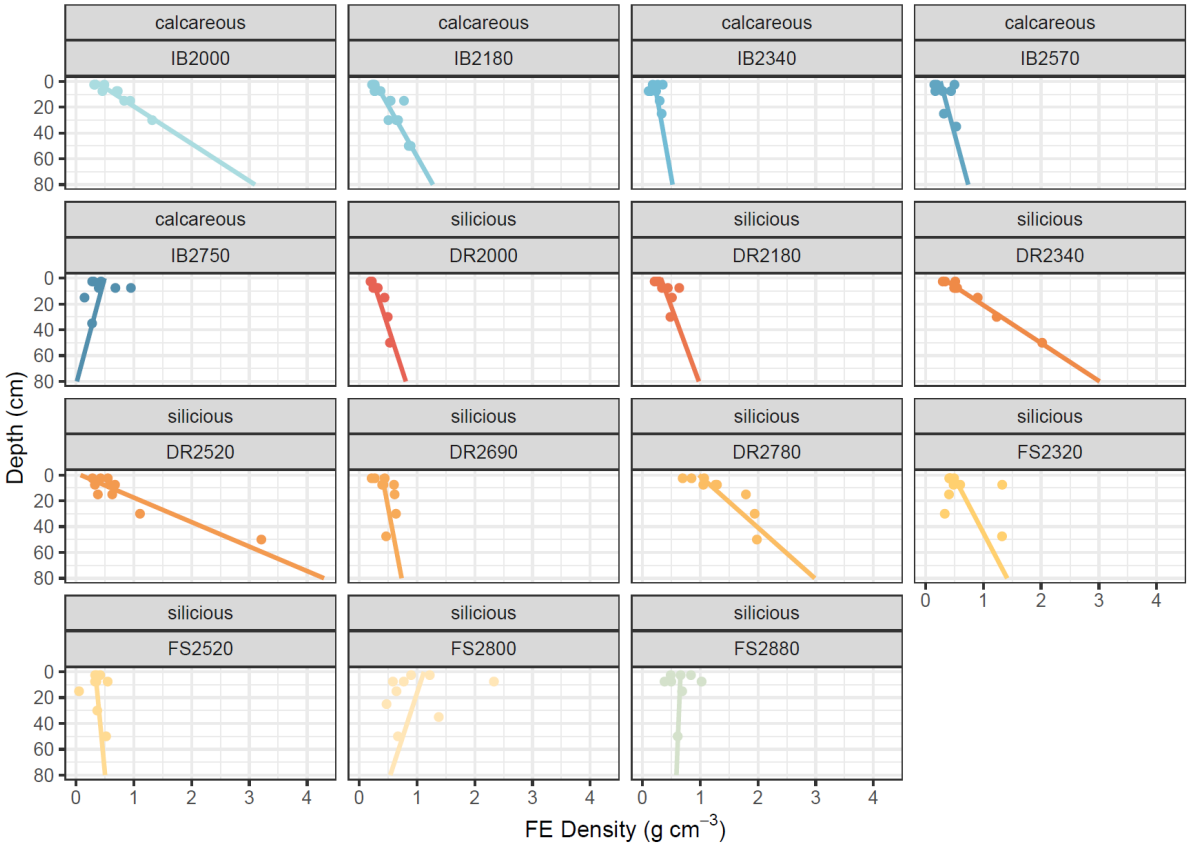

Figure B3: Depth profiles of FE density (g cm^{-3}) across profiles down to bedrock grouped by parent material (calcareous vs. siliceous). Colours indicate sites. Points represent measured FE density values at each depth increment, and lines show the fitted depth trends for each site using linear fits. Note that elevation is indicated by the four-digit site identifiers (e.g., IB2180; 2180 m a.s.l.) while the letters stand for the transect ID.

https://doi.org/10.5194/egusphere-2026-835
Preprint. Discussion started: 16 February 2026

Rock fragment fraction

Rock-fragment fractions increased with depth across all sites and often exceeded 50 % (Figure B4). Depth profiles were consistently characterised by lower coarse-fragment content in the uppermost soil horizons and a steady increase towards the subsoil, in some cases exceeding 70–80 % at greater depths. Linear fits captured these depth trends well across both calcareous and siliceous sites. The intercepts at the surface and the slopes of the depth relationships differed substantially among sites, reflecting differences in soil development, whereby sites at high elevation showed higher rock fractions.

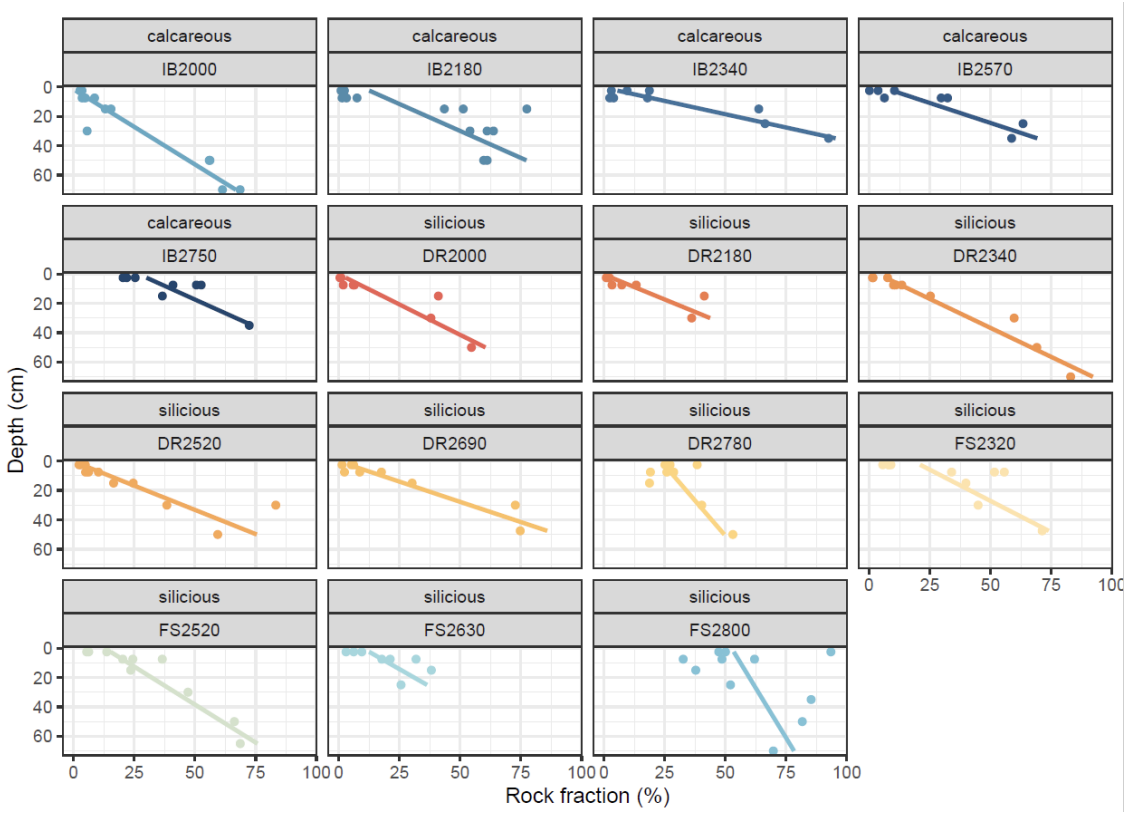

Figure B4: Depth profiles of rock-fragment fraction across all soil pits, grouped by parent material (calcareous vs. siliceous). Colours indicate sites. Points show measured coarse-fragment fractions at each depth increment, and solid lines represent site-specific linear fits describing the increase in rock fraction with depth. Note that elevation is indicated by the four-digit site identifiers (e.g., IB2180; 2180 m a.s.l.).

https://doi.org/10.5194/egusphere-2026-835
Preprint. Discussion started: 16 February 2026

Exemplar PTF workflow with $SOC_{\%}$

At each topsoil sampling site, $SOC_{\%}$ was sampled using soil cores for the intervals 0-5, 5-10, 10-20 cm with four replicates (Figure B5). These measurements define the site's topsoil conditions and provide the starting point for extrapolating $SOC_{\%}$ to greater depths. This example site is located at 2500 m elevation on gneissic bedrock. From the full set of reference soil profiles (n = 18 for $SOC_{\%}$, only those that share key environmental characteristics in respect to elevation and bedrock with the target site are selected as possible fits. To identify sites in a similar elevational range, the profile sites were subset for site within –200 and + 400m. This asymmetric elevation window allows topsoil sites with low SOC to match with low-SOC profiles from higher elevations, which would otherwise not be tested as possible fits. If a completely symmetrical window was chosen, some sites showed a significant mismatch between measured data and fitted profile (data not shown). For this exemplar site, the selected 6 profiles are displayed with thicker lines (Figure B5), indicating that they belong to the same environmental type as the example topsoil site. The exponential decay function from each of the selected profiles is then fitted to the topsoil data, and the best fit is identified based on the RSS and selected as the PTF for $SOC_{\%}$ of this specific topsoil site. In this example, profile DR2520 provided the best fit (Figure B5c). The corresponding exponential curve is then used to compute subsoil SOC stocks based on *Eq. 1*.

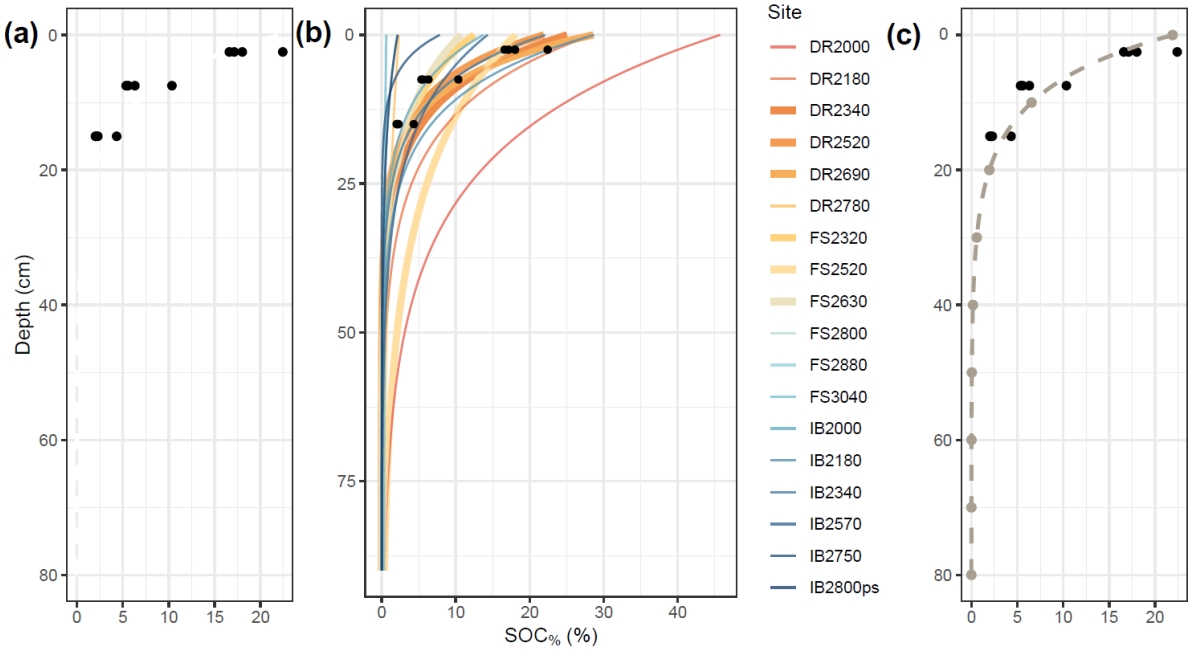

Figure B5: Workflow for selecting environmentally matching profiles and deriving PTF for subsoil $SOC_{\%}$ prediction. a) Measured topsoil $SOC_{\%}$ at the focal site with four replica per depth interval. b) Candidate reference profiles within similar environmental conditions; thicker lines indicate profiles meeting both elevation and bedrock criteria. Colours indicate sites. c) Best-fitting exponential depth function selected from the matching profiles (lowest RSS), applied to predict the subsoil $SOC_{\%}$ trajectory at the focal site.

The same procedure was applied to the parameters FE density and rock fraction for each topsoil site (compare Figure 2).

https://doi.org/10.5194/egusphere-2026-835
Preprint. Discussion started: 16 February 2026

C. Appendix C): Validations of PTF and campaign comparisons

Comparison of PTF-modelled stock vs. profile stocks

To evaluate the reliability of the PTF approach for estimating SOC stocks and the reliability of soil cores in general, we performed two complementary comparisons using soil cores collected immediately adjacent to fully excavated soil profiles. First, total SOC stocks obtained from a combined approach (measured core data for the uppermost 20 cm and PTF-modelled estimates for deeper layers) were compared with fully excavated profile SOC stocks (Figure C1). Second, measured SOC stocks derived from the upper 20 cm of soil cores were compared against SOC stocks calculated from the corresponding excavated profile sections (0-20 cm) to assess consistency between coring and profile-based measurements (Figure C1).

Both comparisons showed strong agreement across the observed range of SOC stocks, indicating that (i) coring provides reliable estimates of topsoil SOC stocks, and (ii) the combination of measured topsoil data with PTF-modelled subsoil estimates yields total SOC stocks consistent with full profile excavations. This supports the use of the PTF-based approach for spatially extensive SOC assessments in alpine terrain, where full profile excavation is logistically infeasible.

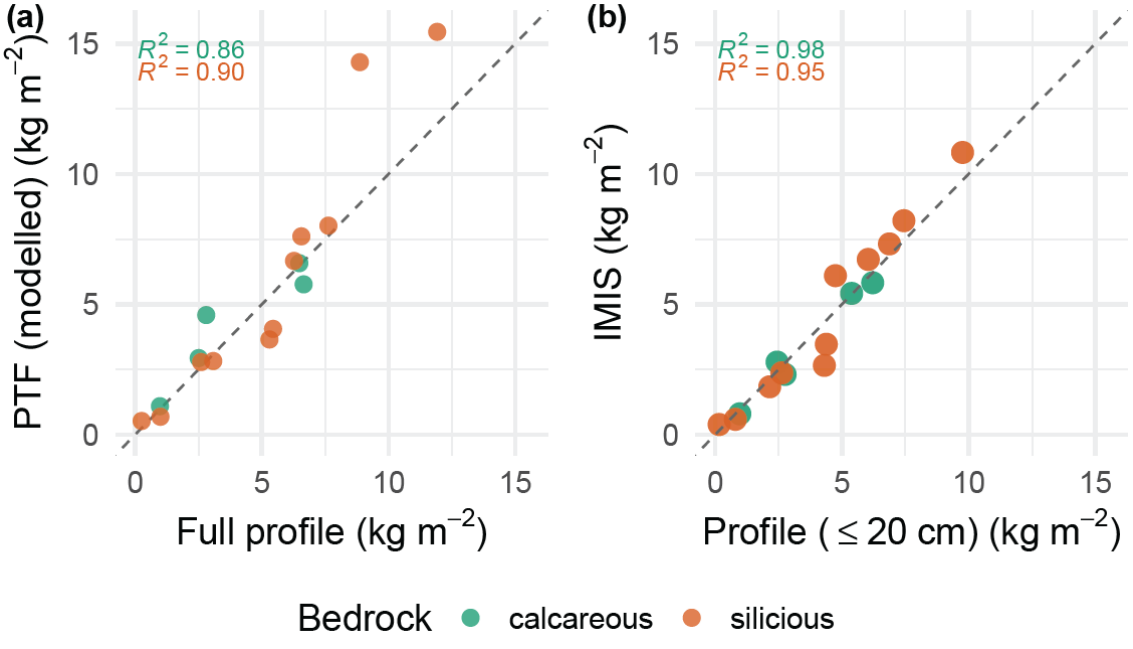

Figure C1: Validation of SOC stock estimates using adjacent soil cores and fully excavated profiles. a) Comparison of total SOC stocks from fully excavated profiles with combined estimates based on measured core data for the upper 20 cm and PTF–modelled subsoil stocks. b) Comparison of SOC stocks derived from the upper 20 cm of soil cores (IMIS) and the corresponding excavated profile sections (0-20 cm). Points represent individual sites, coloured by bedrock type (calcareous vs. siliceous). Dashed lines indicate the 1:1 relationship, and R^2 are shown for each comparison.

https://doi.org/10.5194/egusphere-2026-835
Preprint. Discussion started: 16 February 2026

Comparison of IMIS coring approach with Humax probe

This study combines SOC stock data from two major campaigns (1) Intercantonal Measurement and Information System (IMIS), sampled with an IMIS-corer (diameter: 2 cm), and (2) Biodiversity Monitoring (BDM), sampled with a Humax corer (diameter: 4.8 cm) (Martin Bruch AG, Rothenburg, Switzerland). To assess potential methodological biases in SOC stock estimates due to the two different sampling approaches, we compared data collected at nine sites, which were sampled with the IMIS corer and with the larger Humax corer used in the BDM campaign. The Humax sampling, according to the BDM protocol, is described in Reusser et al. (2023). We further tested linear mixed effect models with site-ID as a random factor and campaign as a fixed effect to investigate possible sampling related differences.

Overall, the high coefficient of determination ($R^2 = 0.80$) indicates strong agreement between the two methods, although deviations from the 1:1 line suggest that, particularly for higher stocks, samples taken with Humax cores during the BDM campaign yield higher SOC stocks (Figure C2a). A site-level comparison of SOC stocks visualized the systematic difference between the two methods (Figure C2b). Linear mixed-effects models indicated that Humax cores from the BDM campaign yielded significantly higher SOC stocks than IMIS cores. On average the difference amounted to 1.62 kg m^{-2} ($p < 0.001$) for the nine sites, where both approaches were used (Table C1: Md. 1).

Table C1: Linear mixed-effects models comparing SOC stocks between both coring methods. Model 1 includes data from the nine sites where both coring approaches were directly compared. Model 2 represents the global dataset across all sites, while Model 3 extends the global model by including elevation and its interaction with coring method. Fixed-effect estimates, 95 % confidence intervals (CI), and p-values are shown. All models include station identity as a random factor to account for the four repeated measurements within sites.

Response	**SOC (kg m^{-2})** *(Md. 1: Nine comparison sites)*			**SOC (kg m^{-2})** *(Md. 2: Global)*			**SOC (kg m^{-2})** *(Md. 3: Global, with elevation interaction)*		
Predictors	*Estimates*	*CI*	*p*	*Estimates*	*CI*	*p*	*Estimates*	*CI*	*p*
(Intercept)	5.32	3.39 – 7.24	**<0.001**	5.70	5.28 – 6.12	**<0.001**	5.41	5.03 – 5.79	**<0.001**
method (IMIS)	-1.62	-2.23 – -1.01	**<0.001**	-1.46	-2.06 – -0.87	**<0.001**	-0.67	-1.20 – -0.14	**0.013**
elevation							-3.53	-4.95 – -2.10	**<0.001**
method (IMIS) × elevation							-2.30	-4.19 – -0.40	**0.017**
n sites	9			287			287		
n Observations	71			1101			1101		

We further extended the analysis across the full dataset of IMIS and BDM sites ($n_{BDM} = 143$, $n_{IMIS} = 144$; $n_{total} = 287$) to check if there was a global bias between the two campaigns (Table C1: Md. 2). As the SOC stocks collected with the IMIS corer were 1.46 kg m^{-2} lower ($p < 0.001$), the estimated global difference matched the offset observed at the nine sites where both coring approaches were used. However, as SOC stocks declined strongly with increasing elevation and the mean elevation of campaigns differs (mean

https://doi.org/10.5194/egusphere-2026-835
Preprint. Discussion started: 16 February 2026

elevation for BDM sites: 2214 m a.s.l., mean elevation for IMIS sites: 2386 m a.s.l), we controlled for the effect of elevation in a third model. After controlling for the elevation difference, SOC stocks measured with the IMIS corer remained significantly lower than those obtained with the Humax corer, although the magnitude of the difference was reduced to 0.67 kg m^{-2} ($p = 0.013$). This indicates that part of the observed method effect reflects differences in the elevational distribution of sampling campaigns, while a residual systematic offset between coring approaches persists – although by less than 1 kg m^{-2}.

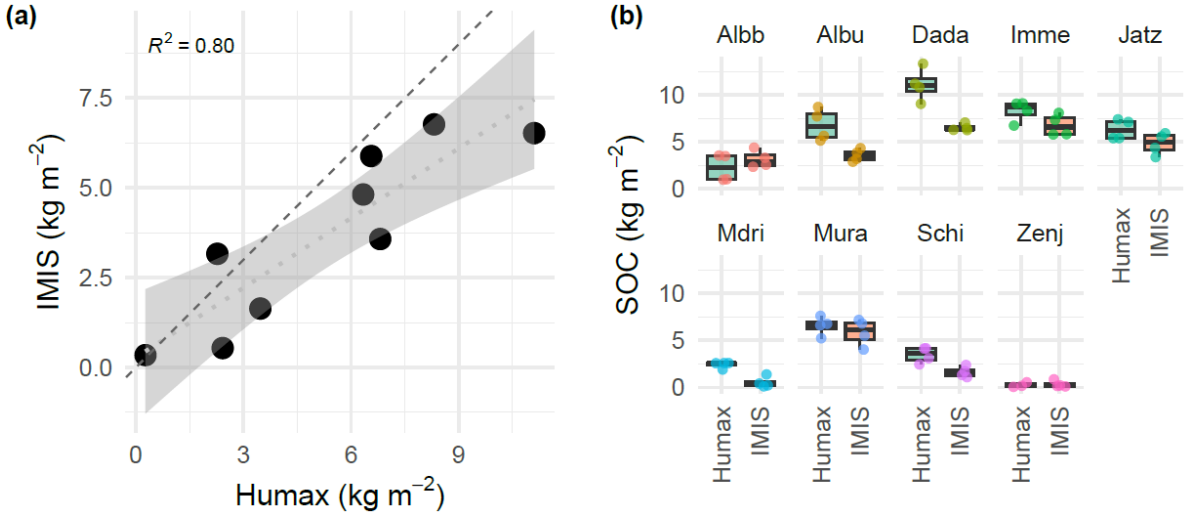

Figure C2: Comparison of SOC stocks estimated using two coring methods; IMIS-corer used in the IMIS campaign, and Humax-corer, which was used in the BDM campaign. a) Site-level comparison of SOC stocks derived from Humax and IMIS cores at nine paired sites. Points represent site means, the dashed line indicates the 1:1 relationship, and dotted line with shaded band shows the fitted linear regression and its 95 % confidence interval ($R^2 = 0.80$). b) Distribution of SOC stocks for each paired site, shown separately for Humax and IMIS cores. Points represent individual replica, and boxplots summarize the within-site variability for each coring method. Colours indicate different sites.

It is possible that differences at paired sites were due to micro-scale in-situ differences as the Humax cores from BDM and the resampled IMIS cores were taken within an area of approximately 25 m^2. More likely, the difference can be explained by differences in the sampling protocol: The BDM campaign aims at collecting four "ideal" soil cores within a pre-defined area (between radius 3 m – 3.5 m) for each site (source: sampling protocol BDM – confidential document by BDM, Version April 2011; also explained in Reusser et al. (2023)) (Figure C3). This approach may lead to an overestimation of FE density and thus SOC stocks. Avoiding rocky areas for sampling ideal soil cores, as was intended in the BDM protocol, alleviates the overestimation of SOC stocks especially at high elevation. Furthermore, when a replicate could not be taken due to sones or roots, only a small fraction of the area (i.e. the ring-shaped area) was effectively probed, while the remaining inner- or outer area may still contain SOC. To reduce this source of uncertainty, we restricted our analysis to BDM sites with at least three replicates, while a mean across the three replica was taken, as it is unclear to what extent the fourth quarter can be considered truly SOC-free. Note, that in the few cases where an incomplete replica was collected (e.g. down to 15 cm), this is noted and considered as SOC-free in our stock calculation – analogous to IMIS samples.

On the other hand, The IMIS sampling approach selected the exact places where cores were taken randomly (Figure C3); if a core hit rock, this was noted as a true zero, reflecting the true amount of FE and SOC arguably better than the average of four Humax

https://doi.org/10.5194/egusphere-2026-835
Preprint. Discussion started: 16 February 2026

cores taken for the BDM campaign. However, the wider corer diameter and thus the larger sampling volume of the Humax probe affects the FE density of the samples: the smaller IMIS corer is more sensitive to the presence of coarse fragments and may underestimate FE density (e.g. when rocks get stuck in the corer), leading to an underestimation of SOC stocks with smaller corer as shown in the direct comparison at nine sites.

The elevational decline of SOC stocks for all samples was steeper for IMIS cores than for Humax cores (Table C1: Md. 3: interaction effect: $estimate_{IMIS:elevation} = -2.3$, $p = 0.02$). Consequently, differences in SOC stocks between coring methods increased with elevation, indicating that Humax-derived SOC stocks increasingly overestimate SOC stocks in high-elevation environments (or IMIS cores underestimate SOC stocks at high elevation). This pattern is consistent with the expected mechanism that small corers may be less representative in coarse, rocky soils (or idealized Humax cores tend to overestimate SOC stocks at higher elevation). However, it is exactly at higher elevations, where the portability of a smaller corer facilitates effective sampling, which ultimately allowed us to cover the whole alpine gradient form treeline to nival regions. We view the possible underestimation of SOC stocks in samples using the IMIS corer as a compromise that reflects a reasonable trade-off between the portability needed to access remote alpine sites and measurement accuracy.

We cannot dismiss the fact that aggregating different sampling campaigns may have lead to some inconsistencies with the data used for spatial modelling. Thus, we acknowledge that, although the use of smaller and lighter IMIS corers enabled the additional sampling of 144 sites, trade-offs contribute to measurement uncertainty. At the same time, we showed that SOC stocks obtained from IMIS cores closely matched those measured in the upper 20 cm of adjacent soil profiles in the previous comparison (Figure C1b). Ultimately, the true SOC stocks likely lie between the estimates derived from the two coring approaches, suggesting that combining spatially random distributed samples in equal proportions provided a pragmatic and robust basis for regional-scale SOC maps.

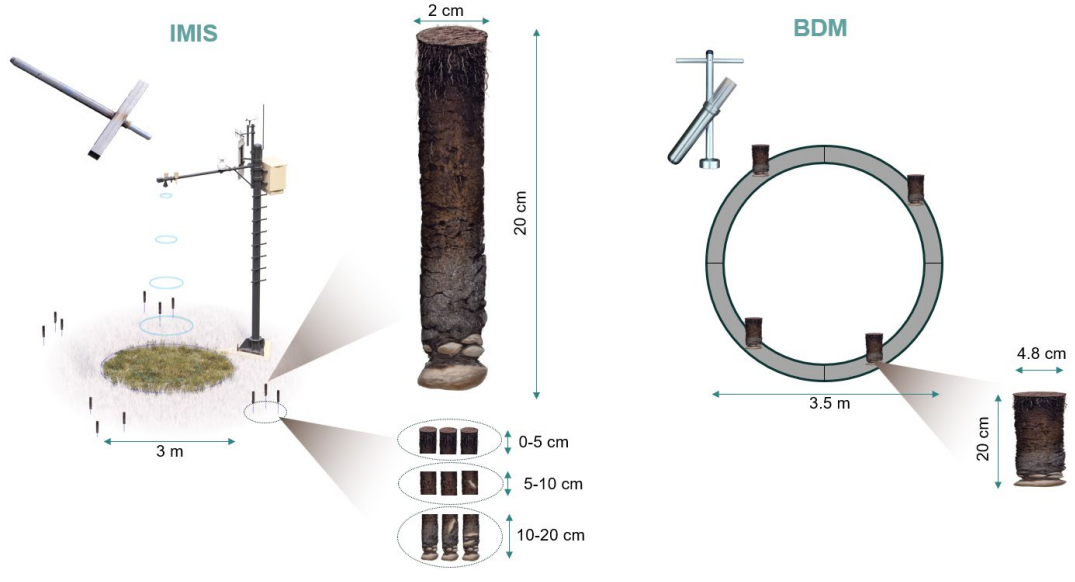

Figure C3: Comparison of the two sampling approaches IMIS (IMIS-corer; diameter 2 cm) and BDM (Humax-corer; diameter: 4.8 cm). For IMIS sites, four spatial replicates were taken, while each replicate consists of three cores placed around a vegetation survey plot of 3 m. The three cores of a replicate were pooled by depth interval 0-5, 5-10, and 10-20 cm. If a core hit rock, this was noted and added to the rock

https://doi.org/10.5194/egusphere-2026-835
Preprint. Discussion started: 16 February 2026

fraction. All IMIS-cores were sampled randomly in each quarter. During the BDM campaign, four Humax cores were collected within a predefined ring-shaped area surrounding each vegetation plot, aiming at a complete 20 cm soil core. If a core could not be extracted as intended, its position was shifted within the ring.

https://doi.org/10.5194/egusphere-2026-835
Preprint. Discussion started: 16 February 2026

D. Appendix D): Spatial cover class categories

Table D1: Cover class reclassification table

Original Cover Class (OBJ_ID / Description) according to swissTLM3D Objektkatalog Vs. 2.3 (03/2025)*	**Reclassified Cover Class**	**Treated in SOC map as**
12 – Wald (forest)	Forest	Excluded
14 – Gehoelzflaeche (wooded area)	Forest	Excluded
6 – Gebueschwald (shrubby forest, mostly *Pinus mugo ssp. mugo*)	Forest	Excluded
1 – Fels (rock; >80 % visible rock) ()	Solidrock	Exposed, bare rock
3 – Felsbloecke (rock blocks ≥80 %)	Solidrock	Exposed, bare rock
5 – Fliessgewaesser (rivers and streams)	water_ice_snow	Excluded
9 – Gletscher (glaciers)	water_ice_snow	Excluded
10 – Stehende Gewaesser (standing waters)	water_ice_snow	Excluded
15 – Schneefeld / Toteis (snow and ice fields)	water_ice_snow	Excluded
11 – Feuchtgebiet (wetlands)	Grassland	Grassland
13 – Wald offen (open forest, with ground covering vegetation)	Grassland	Grassland
8 – Lockergestein locker (loose rocks or scree; 20 % - 80 %, complement: grassland or open soil)	Grassland	Grassland
4 – Felsbloecke locker (loose rock blocks; 20 % - 80 %, complement: grassland or open soil)	Grassland	Grassland
2 – Fels locker (loose rock 20 % - 80 %, complement: grassland or open soil)	Grassland	Grassland
7 – Lockergestein (Scree; >80 % scree)	Scree	(Partly vegetated) Scree
Remaining area	Grassland	Grassland

* https://www.swisstopo.admin.ch/dam/de/sd-web/A3kQ2dAgenqG/2025-03 swissTLM3D 2.3 OK-DE.pdf

1275

https://doi.org/10.5194/egusphere-2026-835
Preprint. Discussion started: 16 February 2026

Depth distribution of SOC stocks by cover class

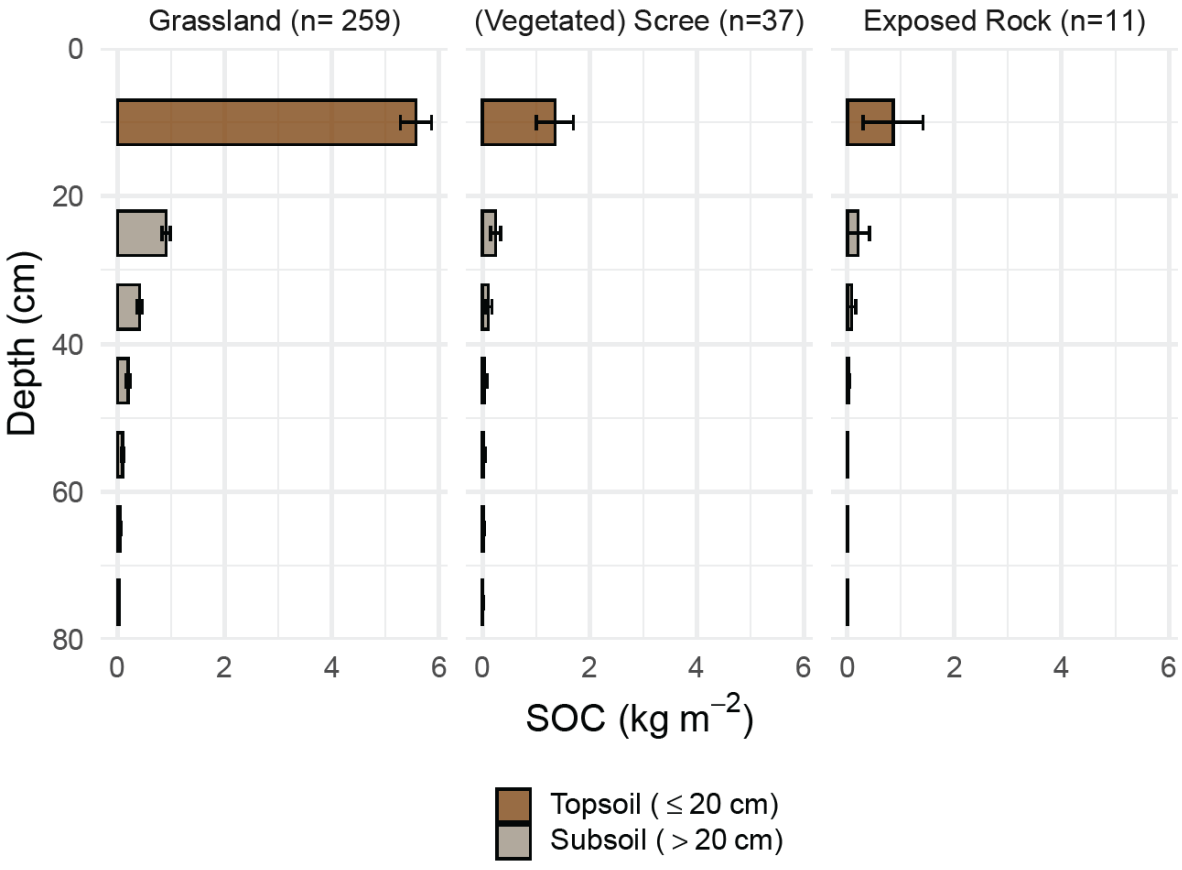

Figure D1: Vertical distribution of SOC by soil depth across the three alpine cover classes: grassland, (partly vegetated) scree, and rocky nival areas. Bars represent mean SOC +- 95 % confidence interval per 10 cm depth interval (20 cm for the topsoil).

1280